

Delivery of mRNA vaccines with heterocyclic lipids increases anti-tumor efficacy by STING-mediated immune cell activation

Lei Miao^{1,2,9}, Linxian Li^{1,2,3,9}, Yuxuan Huang^{1,9}, Derfogail Delcassian^{1,4,5}, Jasdave Chahal¹, Jinsong Han^{1,3}, Yunhua Shi^{1,2}, Kaitlyn Sadtler^{1,4}, Wenting Gao¹, Jiaqi Lin¹, Joshua C. Doloff^{1,2,4,8}, Robert Langer^{1,2,4,6,7} and Daniel G. Anderson^{1,2,4,6,7*}

Therapeutic messenger RNA vaccines enable delivery of whole antigens, which can be advantageous over peptide vaccines. However, optimal efficacy requires both intracellular delivery, to allow antigen translation, and appropriate immune activation. Here, we developed a combinatorial library of ionizable lipid-like materials to identify mRNA delivery vehicles that facilitate mRNA delivery *in vivo* and provide potent and specific immune activation. Using a three-dimensional multi-component reaction system, we synthesized and evaluated the vaccine potential of over 1,000 lipid formulations. The top candidate formulations induced a robust immune response, and were able to inhibit tumor growth and prolong survival in melanoma and human papillomavirus E7 *in vivo* tumor models. The top-performing lipids share a common structure: an unsaturated lipid tail, a dihydroimidazole linker and cyclic amine head groups. These formulations induce antigen-presenting cell maturation via the intracellular stimulator of interferon genes (STING) pathway, rather than through Toll-like receptors, and result in limited systemic cytokine expression and enhanced anti-tumor efficacy.

Vaccination with mRNA is a promising strategy for cancer prevention and treatment. In contrast to DNA vaccines, mRNA vaccination results in transient expression of encoded proteins, and so avoids complications associated with insertional mutagenesis¹. mRNA vaccines can be specifically designed to encode a wide variety of peptide and protein structures, allowing expression of the entire antigen. With a larger number of epitopes presented by class I and class II major histocompatibility complex (MHC), mRNA vaccines can potentially induce a stronger cellular and humoral response than stimulation with peptide antigen vaccines².

A number of clinical trials have explored mRNA vaccination over the past decade³; however, clinical translation has been limited by two major challenges: (1) insufficient intracellular protein expression due to catalytic hydrolysis of mRNA and (2) inadequate antigen loading and maturation of antigen-presenting cells (APCs). To improve mRNA delivery and *in vivo* protein expression, liposomes and polymeric micelle-based formulations are in development, including nanoparticle delivery vehicles made from lipid-like materials^{3,4}.

The design of therapeutics that can carefully balance antigen-specific immune cell maturation and activation, whilst preventing systemic activation of the immune system, remains challenging. There is a growing body of evidence to suggest that adjuvant effects associated with targeted stimulation of type I interferons (IFNs) may support advantageous adaptive immune responses^{1,5,6}. Pathways that can activate IFN secretion have been identified, including Toll-like

receptors (TLRs), retinoic acid-inducible gene-I (RIG-I)-like receptors (RLRs) and stimulator of interferon genes (STING) pathway⁷. Activation of these pathways has been reported to correlate with reduced disease progression and better clinical outcomes in human cancer patients^{8–10}. Recently, involvement of MYD88-dependent TLR signaling pathways (TLR7 or 8) in instigating type I IFN responses has been demonstrated for both mRNA vaccines complexed into DOTMA/1,2-dioleoyl-*sn*-glycero-3-phosphoethanolamine (DOPE) lipoplexes (BioNTech)¹¹ and RNActive (a protamine/mRNA complex by CureVac AG)¹². In addition, cytoplasmic RLRs, including RIG-I and melanoma differentiation-associated protein 5 (MDA5) have also been linked to mRNA-associated inflammation^{13–15}, demonstrating the importance of these innate immune pathways for potentiating the immune response to mRNA vaccine.

Despite this, unspecific activations of innate immune pathways are unsuitable for mRNA delivery. Exogenous mRNA that intrinsically binds to TLRs and RLRs can conversely upregulate protein kinase R, which ultimately inhibits antigen expression and results in a limited antigen-specific immune response¹. Fine-tuning TLR/RLR activation and IFN responses in systems with both mRNA and TLR/RLR agonists remains challenging. mRNAs incorporating chemically modified nucleotides or optimized codon sequences have therefore been developed, and are reported to reduce mRNA-associated immunogenicity⁶.

In an alternative approach, type I IFN secretion can be modulated by co-administering adjuvants (including aluminum salts and

¹David H. Koch Institute for Integrative Cancer Research, Massachusetts Institute of Technology, Cambridge, MA, USA. ²Department of Chemical Engineering, Massachusetts Institute of Technology, Cambridge, MA, USA. ³Ming Wai Lau Centre for Reporative Medicine, Karolinska Institutet, Hong Kong, China. ⁴Department of Anesthesiology, Boston Children's Hospital, Boston, MA, USA. ⁵Division of Regenerative Medicine and Cellular Therapy, University of Nottingham, Nottingham, UK. ⁶Institute for Medical Engineering and Science, Massachusetts Institute of Technology, Cambridge, MA, USA. ⁷Harvard-MIT Division of Health Science and Technology, Massachusetts Institute of Technology, Cambridge, MA, USA. ⁸Present address: Departments of Biomedical & Materials Science Engineering, Translational Tissue Engineering Center, Wilmer Eye Institute and the Institute for NanoBioTechnology, Johns Hopkins University School of Medicine, Baltimore, MD, USA. ⁹These authors contributed equally: Lei Miao, Linxian Li, Yuxuan Huang. *e-mail: dgander@mit.edu

TriMix mRNA¹⁶) that target other immune cell activation pathways, or by altering mRNA delivery kinetics via optimized vaccine administration^{11,17}. Recently, the STING signaling pathway has emerged as a TLR/RLR-independent mediator of the host innate immune response¹⁸. Additionally, small-molecule or polymeric STING activators have been reported to induce relatively low levels of local and systemic inflammation when used as adjuvants, as compared with TLR agonists^{19–23}. A number of small-molecule STING agonists are currently in clinical trials^{9,24}; however, their success has been limited due to the challenges of cytosolic delivery of these molecules^{25,26}.

Here, we present a systematic study of lipids that can simultaneously mediate mRNA delivery and provide targeted adjuvant stimulation via the STING pathway. A library of these lipids is developed using a one-step three-component reaction (3-CR)²⁷. This strategy increases the diversity of synthesized lipid structures, and facilitates identification of structure–function relationships. Using this approach, we have identified the head group as a key component; changing the chemical structure of the lipid head group allows us to tune the immunostimulatory effect of these lipids. We further show that lipids with cyclic amino head groups activate the MYD88 (that is, TLR7 or 8)/RLR (RIG-I and MDA5)-independent STING pathway. Moreover, the STING-activatable cyclic lipids were condensed with mRNA to formulate lipid nanoparticles (LNPs). Cellular internalization can thus be improved through nanoparticle-mediated endocytic mechanisms^{28,29}, further improving the intracellular activation of STING pathways^{25,30}. This study provides evidence of lipid adjuvant-assisted mRNA vaccination, using LNPs designed to efficiently deliver mRNA and simultaneously activate the immune system through an mRNA-independent STING pathway.

Results

Design and synthesis of a lipid library. We designed an isocyanide-mediated 3-CR to simultaneously couple primary or secondary amines³¹, ketones³² and isocyanides or isocyanide derivatives³³ (Fig. 1a). The structures are composed of alkyl and alkylene ketone lipid tails, isocyanide linkers and amine head groups (Fig. 1b). Using this 3-CR, we synthesized a pilot library of 1,080 lipids (Fig. 1c) containing combinations of the following substructures: (1) varied alkyl chain lengths from C6 to C18, with different degrees of saturation³⁴; (2) side chains coupled to the lipid tail via imine, amide and 2,5-dihydroimidazole groups; (3) degradable isocynoacetate ester bonds in selected side chains; (4) polar head groups containing primary or secondary amines, with the distance between amines varied from two to three carbons; and (5) polar head groups containing hydroxyl groups or cyclic structures³⁵. We used the unique chemistry of isocyanides to couple these lipids in a one-pot, high-throughput reaction using polar, protic solvents (ethanol and propanol)³⁶. The isocyanides chosen in this reaction scheme can function as both electrophiles and nucleophiles, and therefore offer advantages over conventional lipids synthesized using multi-step reactions^{3,35,37,38} which require toxic catalysts, solvent exchange and protection/deprotection steps (Supplementary Note 1 lists synthesis and characterization details)³³. This three-dimensional combinatorial approach facilitated simple and rapid synthesis of a large and diverse library of materials, with which we tested mRNA delivery efficiency³⁵.

Lipid-mediated mRNA delivery in vitro and in vivo. Effective mRNA vaccination requires both efficient intracellular antigen expression and subsequent immune cell activation to generate a robust immune response. We first evaluated the mRNA delivery efficacy of our lipid library by loading firefly luciferase (Fluc) mRNA (mLuc) into LNPs and comparing luciferase protein expression in cell lines. These LNPs were composed of a lipid mixture containing one of the synthesized ionizable lipids, helper lipid, cholesterol and 1,2-dimyristoyl-*sn*-glycero-3-phosphoethanolamine-*N*-[methoxy-(polyethyleneglycol)-2000] (ammonium salt) (C14-PEG) (Fig. 1d,e)³⁹.

Results in HeLa cells are shown in Fig. 2a. Lipid treatments that showed cell viability <80% were eliminated from future studies (Supplementary Fig. 1). Of the 1,080 lipid members, 969 lipids demonstrated improved mRNA transfection efficiency compared with naked mRNA. Of these, 232 lipids increased luciferase expression to over 10,000 units (Supplementary Fig. 1). Analysis of these 232 lipids revealed that mRNA delivery and protein expression was generally enhanced in lipid systems containing longer alkyl chains with reduced saturation (Fig. 2b). The inclusion of an ester group in the lipids appeared to enhance delivery efficiency (that is, Iso 4–6; Fig. 2c), whereas adding a hydroxyl group to the lipid head, in most cases, decreased delivery efficacy (that is, A10; Fig. 2d). Next, we tested mLuc delivery to primary APCs known to be important in vaccine therapeutic efficacy. A range of lipids containing the ketone 2DC18 were formulated into LNPs and used to deliver mLuc to mouse bone marrow-derived dendritic cells (BMDCs) and macrophages (BMDMs). Our results suggest that delivery efficiency is similar in BMDCs, BMDMs and HeLa cells, and we identified A2-Iso5-2DC18 and A12-Iso5-2DC18 as the most potent mRNA delivery vehicles across these three cell types (Fig. 2e–g).

We next explored the in vivo delivery efficacy of these candidate lipids, using two different helper lipids, DOPE and 1,2-distearoyl-*sn*-glycero-3-phosphocholine (DSPC), to formulate LNPs^{39,40}. Fusogenic DOPE enhanced delivery compared with DSPC and was therefore chosen for the remainder of the LNP formulation studies (Supplementary Fig. 2). LNPs from all lipids in the library were individually prepared, and lipids were classified into one of nine groups based on their ketone structure. LNPs with the same ketone structure were mixed immediately before injection, and delivered using intramuscular or subcutaneous injection to mimic typical clinical vaccination approaches^{20,41,42}. These nine groups each contained a mixture of LNPs with a conserved ketone structure and various other functional groups. Consistent with our in vitro data, this screen revealed that longer, unsaturated alkyl tails increased delivery efficacy (Fig. 2h). We identified 2DC18 ketone derivatives as the most efficacious, and so further categorized 2DC18 lipids based on their isocyanide substructure (Fig. 2i). We noted that isocynoacetate lipids (butyl, ethyl or methyl) enhanced mRNA delivery compared with lipids synthesized using the conventional isocyanide. We therefore classified lipids containing ethyl isocynoacetate and 2DC18 ketones as optimal substructures for lipid mRNA delivery (Fig. 2j). Using this batch screening and analysis method substantially reduced the number of animals, time and cost required to screen all 1,000 compounds in our lipid library and allowed us to confirm A2-Iso5-2DC18 and A12-Iso5-2DC18 as the top-performing lipids for both subcutaneous and intramuscular injection (Supplementary Fig. 3), consistent with the in vitro cell-based studies. These lipids contain several structural similarities: (1) two amines in the polar head group, spaced three carbons apart; (2) no hydroxyl group; and (3) the presence of at least one tertiary amine.

Top-performing lipids exhibit different anti-tumor immunity. Dihydroimidazole-linked lipids A2-Iso5-2DC18 and A12-Iso5-2DC18 screened from the library have been identified and purified as the top-performing lipids for mRNA delivery (Supplementary Note 2 and Fig. 3a). Formulation of LNPs has also been optimized (Supplementary Note 3, Supplementary Table 1 and Supplementary Fig. 4)^{39,43}. Separately, decreasing lipid tail saturation is thought to increase transfection efficiency through enhanced fusogenic H_{II} phase formation^{34,44}. To determine whether this approach could enhance delivery in our system, we compared ketones with two (2DC18) or four (4DC19) double bonds in the lipid tail. LNPs exhibited comparable particle size, encapsulation efficiency and protein expression levels (statistically no difference) between systems with two or four double bonds in the lipid tail (Supplementary Fig. 5).

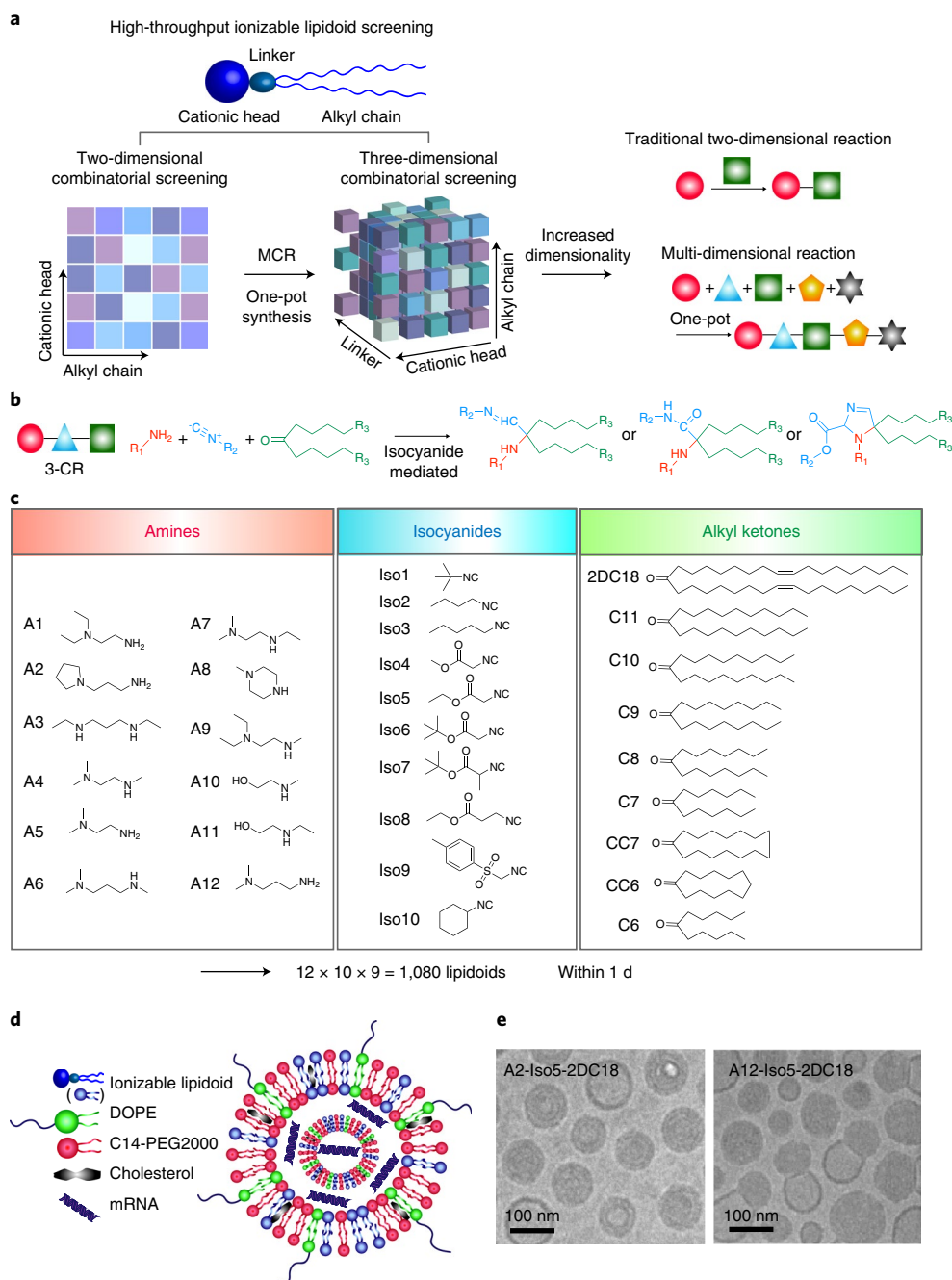


Fig. 1 | Isocyanide-mediated 3-CR for high-throughput synthesis of lipidoids. **a**, A schematic to illustrate the advantages of using a three-dimensional combinatorial synthesis library compared with a traditional two-dimensional combinatorial library. **b**, Proposed reaction mechanisms of the isocyanide-mediated one-pot reaction. **c**, Structures of the three components of the lipidoid (amine, isocyanide and ketone) used in the synthesis library are shown. **d**, Schematic of mRNA-encapsulating LNPs. **e**, Representative cryogenic electron microscopy images of LNPs. Multi-lamellar mRNA-loaded LNPs are shown in the images. MCR, multi-component reaction.

We next tested the vaccination potential of our lead lipids (A2-Iso5-2DC18 and A12-Iso5-2DC18, referred to as A2 and A12, respectively) following subcutaneous injection^{45,46}. We found that both the A2- and A12-loaded mLuc LNPs could induce protein expression in the local injection site and the draining lymph nodes (Fig. 3b–e). To determine whether APCs were transfected within lymph nodes, we delivered Cre-recombinase mRNA LNPs (mCre) to the Ail4D reporter mouse model. These mice harbor a mutation in the Gt(ROSA)26Sor locus and cells co-express tdTomato on injection of mCre (Fig. 3f). Our results indicated that the A2 and A12 LNPs induced similar levels of protein expression

and were able to transfect central APCs including macrophages/monocytes (CD11b⁺) and dendritic cells (CD11c⁺) (Fig. 3g and Supplementary Fig. 6).

We then tested the adaptive immune response and anti-tumor efficacy of our mRNA lipid delivery systems using the Ovalbumin (OVA)-expressing B16F10 mouse melanoma model and an OVA mRNA (mOVA) vaccine. We found that the A2 mOVA LNPs induced a significantly higher antigen-specific cytotoxic T lymphocyte (CTL) response compared with the A12 mOVA LNPs, in parallel with robust IFN- γ secretion (Fig. 3h and Supplementary Fig. 7). Additionally, the A2 mOVA LNPs vaccines induced robust

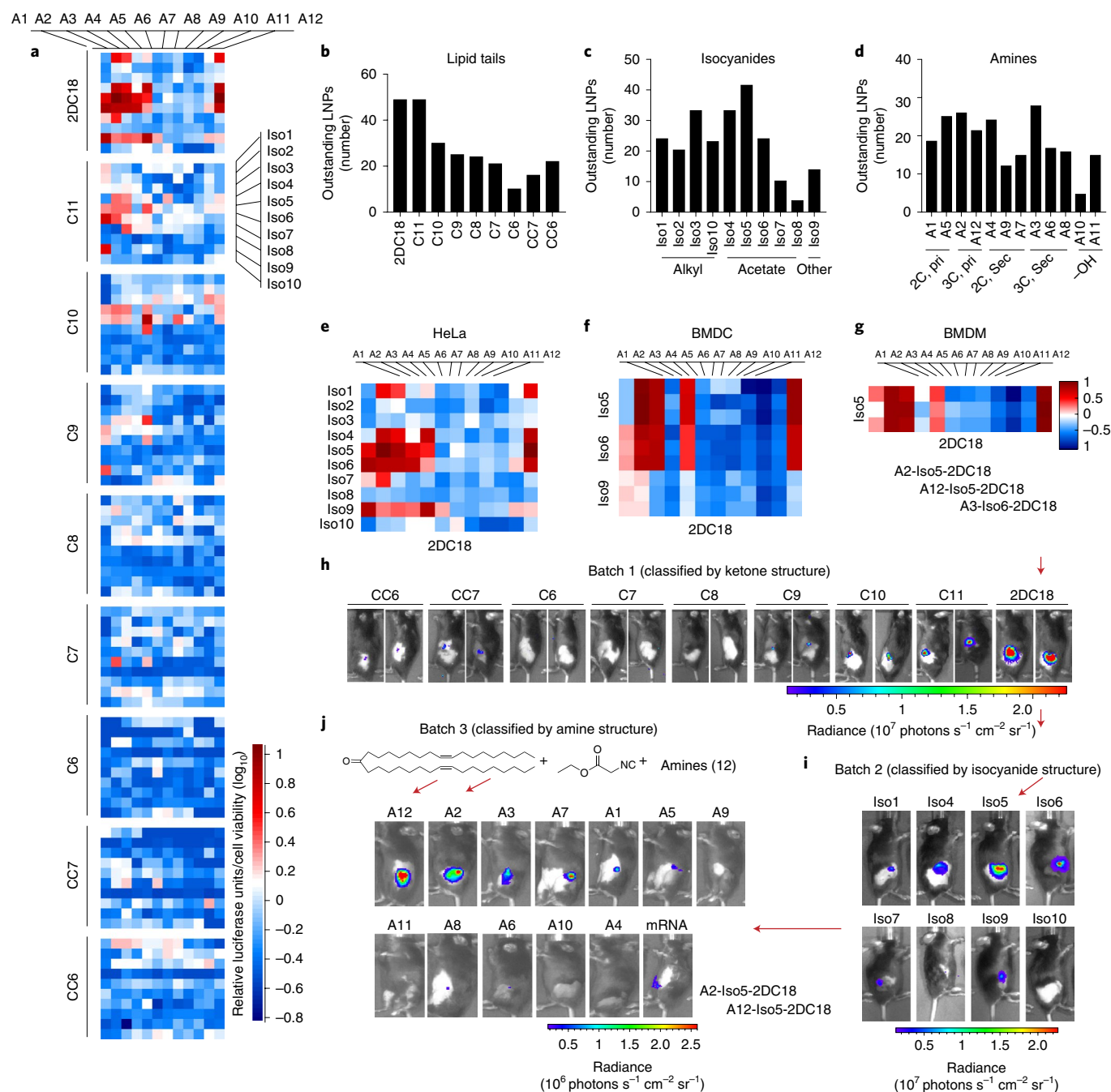


Fig. 2 | In vivo and in vitro screening of lipidoids for Fluc mRNA (mLuc) delivery. **a**, HeLa cells were treated with mLuc-loaded LNPs. The relative luciferase expression/cell viability after incubating with mLuc LNPs overnight is shown in a heat map. **b-d**, Analyses of lipid tail (**b**), isocyanide (**c**) and amine (**d**) structures by transfection efficiency, quantified for the 232 lead candidate lipids highlighted from Supplementary Fig. 1. In **d**, pri indicates that the end group is a primary amine; sec, end group is a secondary amine; 2C, two carbons between the two nitrogen-containing groups; 3C, three carbons between the two nitrogen-containing groups; -OH, end group is a hydroxyl. **e-g**, Forty-eight lipids with 2DC18 tails, Iso4, 5, 6 and 9, were screened in HeLa cells (**e**), BMDCs (**f**) and BMDMs (**g**). The three top-performing lipids are listed. Lipids are named as amine-isocyanide-ketone. The relative luciferase expression was calculated by setting the median expression level of lipids as \log_{10} in each cell line ($n=3$ independent experiments per group). **h-j**, Schematic and results of the in vivo batch analysis, where batch 1 analysis determined the optimal ketone structure (2.5 mg kg^{-1} mLuc, 120 LNP mixtures per mouse) (**h**); batch 2 analysis identified the optimal isocyanide structure (0.75 mg kg^{-1} , 12 LNP mixtures per mouse) (**i**); and finally batch 3 identified the top-performing individual lipids (0.5 mg kg^{-1} mLuc per mouse) (**j**). All of the in vivo studies in **h-j** were dosed through subcutaneous injection ($n=2$ biologically independent mice per group, initial screening). Both in vitro and in vivo screenings were repeated twice independently with similar results.

tumor suppression with only two doses (once per 5 d) (Fig. 3i), whereas the A12 mOVA LNPs showed almost no anti-tumor efficacy in the B16F10-OVA mouse melanoma model. When the A2 mOVA LNPs were codelivered with an anti-PD1 antibody, this combination therapy significantly retarded tumor growth and

improved overall survival (Fig. 3j,k). The number of systemic and tumor-infiltrating antigen-specific T cells also increased dramatically (20–30-fold) following A2 vaccination using our mOVA or mOVA/anti-PD1 combination vaccination approach (Fig. 3m,n and Supplementary Fig. 8).

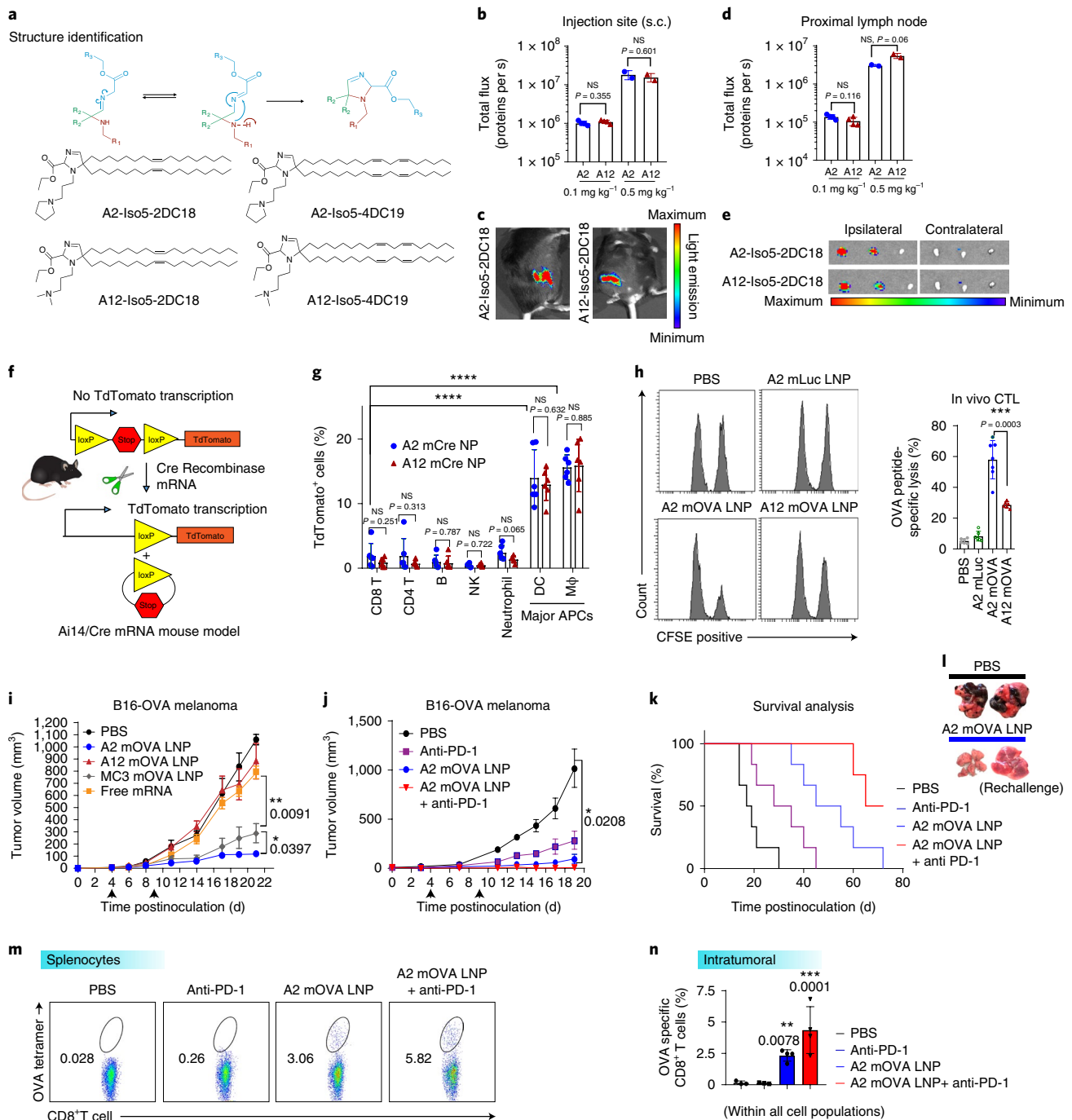


Fig. 3 | Top-performing lipidoids exhibit different anti-tumor immunity. **a**, A schematic of the structure of the top-performing lipidoids. **b,d**, Quantification of Fluc protein expression in local injection site (**b**) and draining lymph nodes (LNs) (**d**). Female B6 mice were dosed with 0.1 mg kg^{-1} mLuc ($n=4$ biologically independent mice per group) and 0.5 mg kg^{-1} mLuc per mouse ($n=2$ biologically independent mice per group), respectively. A2 and A12 LNP treatment groups were compared using unpaired two-tailed Student's *t*-test. **c,e**, One of the representative images of Fluc expression (**c**) and distribution locally and in the lymph nodes (**e**) (dosed at 0.1 mg kg^{-1} mRNA). **f**, A schematic of the Ai14/Cre mRNA mouse model. **g**, FACS quantification of tdTomato-positive cells expressed in lymph nodes 48 h after injection of mCre LNPs (0.5 mg kg^{-1} mCre per mouse). NK, natural killer cells; DC, dendritic cells; M Φ , macrophages/monocytes; APC, antigen-presenting cells. mRNA is mainly expressed in macrophages/monocytes and dendritic cells ($n=6$ biologically independent mice per group, unpaired two-tailed Student's *t*-test). **h**, An in vivo CTL assay of mOVA-loaded LNPs was performed 5 d after second injection ($15 \mu\text{g}$ mOVA per mouse). CTL, cytotoxic T lymphocyte assay; OVA, ovalbumin; mLuc, mRNA encoding firefly luciferase; CFSE, carboxylfluorescein diacetate succinimidyl ester cell-labeling dye. Quantification is shown on the right ($n=6$ for PBS, A2 and A12 mOVA groups and $n=7$ for A2 mOVA group). Biologically independent mice were used in each group; data were analyzed by one-way ANOVA and Tukey's multiple comparisons test). **i-k**, Tumor volume was measured following mOVA-loaded LNP vaccination using $15 \mu\text{g}$ mRNA (**i**), administered once per week for the first 2 weeks (arrows), or in combination with anti-PD1 antibody (**j**) and overall survival plotted (**k**); anti-PD-1, anti-programmed cell death protein 1 antibody ($n=6$ biologically independent mice per group, two-way ANOVA repeated measures and Tukey's multiple comparisons test). **l**, Mice were rechallenged on day 15 with an intravenous injection of tumor cells (2×10^5), and lung metastasis was evaluated 21 d later. **m,n**, CD8⁺ T cells were isolated from splenocytes (**m**) and within tumor regions (**n**) and stained with OVA tetramer before FACS analysis 5 d after the repeat injection ($n=4$ biologically independent mice per group, one-way ANOVA and Tukey's multiple comparisons test). Data are represented as the mean \pm s.d. * $P < 0.05$, ** $P < 0.01$, *** $P < 0.001$. NS, not significant; s.c., subcutaneous.

Finally, using a tumor rechallenge model, we examined the durability of T-cell responses following vaccination with A2 mOVA LNPs. Mice were able to efficiently eliminate B16-OVA cells following intravenous vaccination (Fig. 3l), demonstrating long-lived protection against tumor challenge. Although the A2 and A12 LNPs demonstrated similar mRNA delivery efficacy to local lymph nodes and APCs, only the A2 LNP system was able to induce robust tumor immunity.

A lipid library to identify immune-stimulatory structures. The major structural difference between A2 and A12 lipids is the amino head group; A2 contains a heterocyclic amine whereas A12 contains a linear amine. We therefore explored structure–function relationships in lipid design, specifically investigating whether the nature of the head group (heterocyclic versus linear) affects lipid-associated immunogenicity. We generated a second lipid library with conserved 2DC18 and ethyl isocanoacetate moieties, but varied the amine components to include either linear tertiary amines or heterocyclic tertiary amines (Fig. 4a and Supplementary Table 3). We used these lipids to formulate LNPs with similar particle size, encapsulation efficiency and comparable mRNA delivery efficiency, and compared IFN- γ expression following mOVA vaccination (Fig. 4b).

Lipids containing heterocyclic groups (cyclic lipids) showed significantly increased IFN- γ secretion compared with lipids containing linear tertiary amines (linear lipids) (Fig. 4c). In particular, LNPs containing the lipid A18 increased IFN- γ -positive secretion in splenocytes approximately 10-, 4- and 75-fold compared with MC3-based LNPs (Fig. 4c), one of the lipid materials currently US Food and Drug Administration-approved for RNA delivery³, and in-house-generated A2 and A12 LNPs (Fig. 4c,d), respectively. In contrast, treatment with free mRNA, peptide or recombinant OVA protein failed to induce a T-cell response, and T-cell responses were minimal even when these agents were combined with a known TLR-4 agonist, lipopolysaccharide (LPS) (Fig. 4c). Notably, codelivery of empty A18 LNPs with free OVA peptide improved this T-cell response, demonstrating that the lipid A18 has intrinsic stimulatory effects; we identified CD8⁺ T cells as having a leading role in orchestrating the IFN- γ secretion (Supplementary Fig. 9). We then measured the OVA-specific CTL response associated with these LNPs. We found that cyclic lipids increased OVA-specific splenocyte death, with A17, A18 and A21 LNPs able to reduce the number of OVA peptide-pulsed splenocytes by 98% (Fig. 4e–g). We also examined the durability of T-cell responses; we found that CD8⁺ T cells were greatest on day 10 (~20%) following administration of mRNA A18 LNPs on day 1 and day 6, and that cells were able to kill up to 50% of the peptide-pulsed splenocytes on day 40 (Fig. 4h,i and Supplementary Fig. 10). Mice immunized with A17, A18 and A21 LNPs showed OVA-specific serum IgG antibody titers over 2.5-fold higher than mice treated with MC3 LNPs (Fig. 4j). Next, we examined the importance of this cyclic head group for immune cell activation.

Cyclic lipids stimulate adaptive immune cells through STING.

Using our second-generation lipid library, we investigated protein expression in vivo following mLuc vaccination (Supplementary Fig. 11a–c). The majority of lipids exhibited similar protein expression levels (more than two times higher than that of LNPs formulated with commercially available Dlin-KC3-DMA). We noted that LNPs formulated with A18 or A21 (containing a piperidinyll six-member and an azepanyl seven-member side chain, respectively) significantly enhanced delivery efficacy. Protein expression was also observed in macrophages and monocytes, as seen for the A2 and A12 LNPs tested earlier (Fig. 3g), suggesting that the A18 and A21 LNPs induce robust antigen expression in several key immune cells.

To test the ability of our second-generation LNPs to directly activate APCs (Fig. 5a)^{47,48}, we treated naïve BMDCs for 24 h with cyclic LNPs or linear LNPs containing mOVA. We selected lipids with comparable mRNA delivery efficiency (cyclic, A2 and A13; linear, A12 and A24) and used 5-methoxyuridine-modified mOVA to further reduce mRNA immunogenicity, ensuring that we compared the immunostimulatory effect of the lipid structure. We found that mRNA encapsulated in cyclic LNPs increased expression of dendritic cell activation markers (CD40, MHCII) 2–3-fold compared with linear LNPs (Fig. 5b,c). Notably, empty cyclic LNPs were also able to upregulate these activation markers (Supplementary Fig. 12), clearly indicating that the activation of APCs is not only triggered by mRNA, but also by the unique structural features of this class of cyclic lipids. Similar trends were seen in vivo, where CD86/CD40 expression was upregulated in dendritic cells collected from the draining lymph nodes of mice treated with cyclic LNPs compared with mice treated with linear LNPs (Fig. 5d,e). We noted some differences in delivery efficacy, dendritic cell activation and T-cell responses among the cyclic lipids, suggesting that the exact lipid structure plays an important role in fine-tuning the overall immune response.

Given the importance of type I IFNs in APC activation and generation of a robust T-cell response, we next examined IFN-stimulated gene (ISG) expression in lymph nodes following mOVA LNP vaccination. Cyclic lipids were able to elicit upregulation of IRF7, CXCL10 and IFN β 1 d postinjection, but this expression was transient and decreased to background levels over the subsequent 5 d (Fig. 5f,g and Supplementary Fig. 13). mRNA delivery has been reported to activate type I IFN-mediated immune responses through the TLR-MYD88 pathway¹¹. Moreover, single-stranded RNA and double-stranded RNA bearing a 5' triphosphate are known to be recognized by RIG-I and MDA5 (ref. 49). Additionally, there is emerging evidence that some polymeric materials may also activate innate immune responses through the STING pathway^{20,23}. We therefore examined the potential mechanisms of type I IFN activation of our lipids, using CDS reporter cell lines (InvivoGen) with stable knockout (KO) of *Myd88*, *Mda5*, *Rig-I* (*Ddx58*) and *Sting* genes. Using cGAMP (STING-dependent) and LPS (TLR-dependent) controls, we demonstrate that in wild-type cells, cyclic mOVA LNPs significantly facilitated IRF activation compared with linear LNPs (Fig. 5h and Supplementary Fig. 14). IRF activation was slightly reduced in *Mda5* KO, *Rig-I* KO and *Myd88* KO cells treated with cyclic mOVA LNPs; however, it was entirely absent in *Sting* KO cells, demonstrating that the STING pathway governs the lipid-based adjuvant effect of cyclic LNPs (Fig. 5h).

To further validate the activation of the cyclic GMP-AMP synthase (cGAS)-STING-type I IFN pathway by cyclic LNPs, we isolated BMDCs from *Sting^{g1/g1}*, IFN receptor (*Ifn- $\alpha\beta$ ^{-/-}*) KO and wild-type mice and examined ISG upregulation and APC activation using two cyclic LNPs (A2 and A18) and two linear LNPs (A12 and A25) (Fig. 5i,j and Supplementary Fig. 15). Cyclic and linear lipids with similar numbers of carbon in the head groups were compared (A2 similar to A12, A18 similar to A25). These four lipids were used for the rest of the representative studies unless stated otherwise. Consistent with mRNA level changes in wild-type mice (Fig. 5g), we observed elevated secretion of CXCL10 protein in the supernatant of wild-type BMDCs, but not in *Sting^{g1/g1}* and *Ifn- $\alpha\beta$ ^{-/-}* BMDCs 24 h after co-incubating with cyclic LNPs. We also noted that BMDCs isolated from wild-type mice matured when treated with cyclic LNPs (empty or containing mRNA) (Fig. 5j and Supplementary Fig. 15), but this was not observed in BMDCs isolated from *Sting^{g1/g1}* and *Ifn- $\alpha\beta$ ^{-/-}* animals. In contrast, the linear LNPs were unable to elicit a strong STING-type I IFN activation and APC maturation in any of the models tested, confirming that the additional adjuvant effect is specific to cyclic LNPs, and is mediated by the STING pathway.

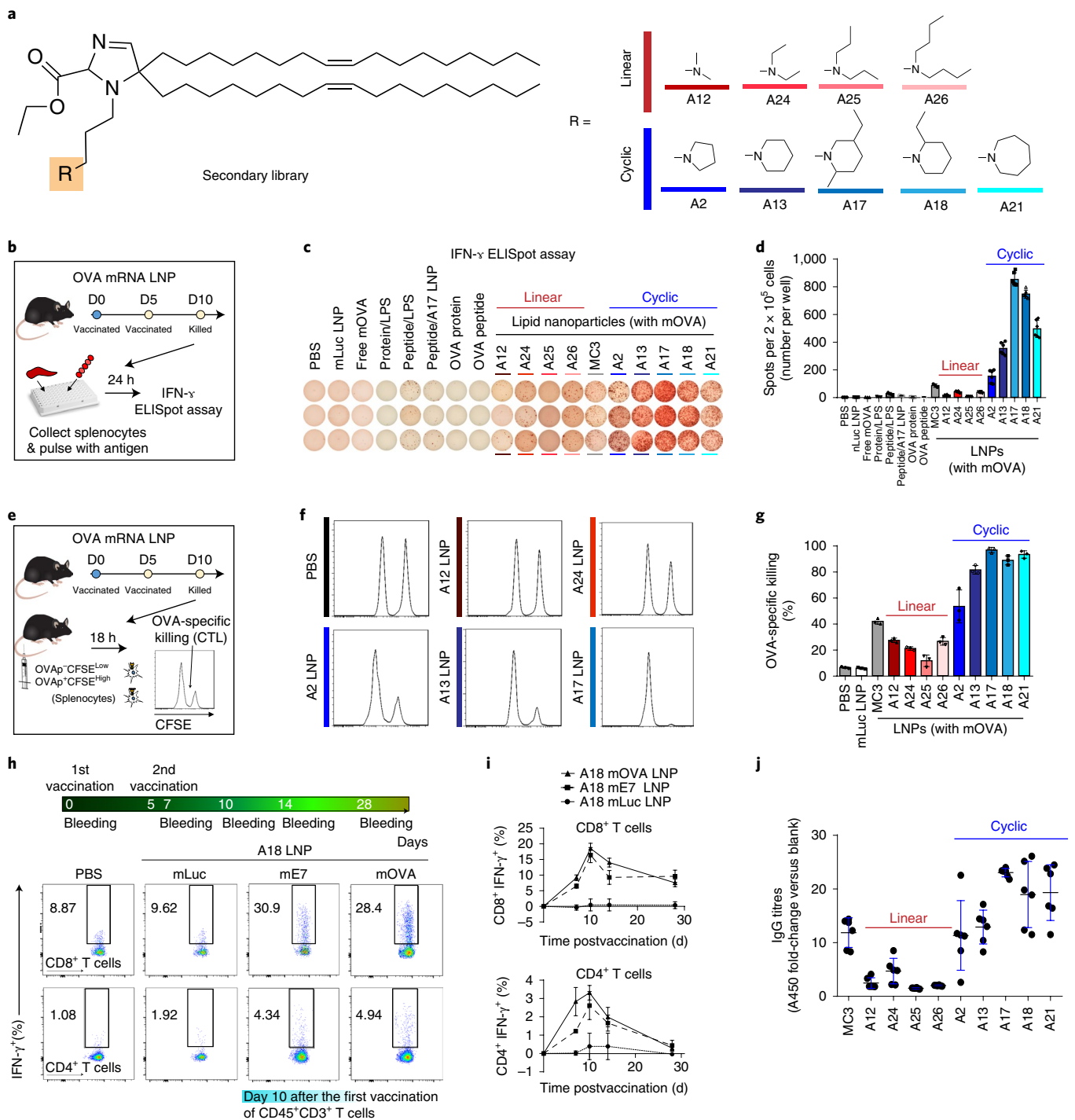


Fig. 4 | Heterocyclic amine-containing lipidoids act as mRNA vaccines with robust antigen-specific T-cell and humoral responses. **a**, A schematic of the structure for the second lipidoid library, where R is one of four linear amines or one of five heterocyclic amines. **b–d**, Enzyme-linked immunospot (ELISpot) analysis of IFN- γ -spot-forming cells among splenocytes after ex vivo re-stimulation with SIINFEKL peptide on day 10 in different nanoparticle-treated groups ($15 \mu\text{g}$ mOVA per mouse, $n=6$ biologically independent mice per group for cyclic and linear LNPs, $n=3$ biologically independent mice per group for control groups). **e–g**, CTL analysis of vaccinated mice ($n=3$ biologically independent mice per group). **h,i**, Representative FACS analysis of IFN- γ expression in CD4 $^+$ T cells and CD8 $^+$ T cells at indicated time points (data were subtracted by PBS treatment at day 0). Results demonstrate long-lived CD8 $^+$ T-cell response ($n=3$ biologically independent mice per group). **j**, OVA-specific production of IgG in response to mOVA vaccination in various LNPs ($n=6$ biologically independent mice per group). Data are presented as mean \pm s.d. D, day.

Furthermore, the adaptive immune response in *Sting*^{tg/tg}, *Myd88*^{-/-} and *Mavs*^{-/-} (downstream adapter of RIG-I and MDA5) or *Ifn- α br*^{-/-} mice demonstrated that adaptive T-cell responses (IFN- γ enzyme-linked immunospot (ELISpot)) were almost eliminated in *Sting*^{tg/tg} and *Ifn- α br*^{-/-} mice treated with cyclic LNPs (A2 and A18).

T-cell responses were still observed following KO of TLR-MyD88 or RIG-I/MDA5-MAV pathways, suggesting that the STING pathway is the key mediator of this effect (Fig. 5k). In contrast, the linear LNPs (A25) were unable to elicit a strong IFN- γ response in any of the models tested (Fig. 5k).

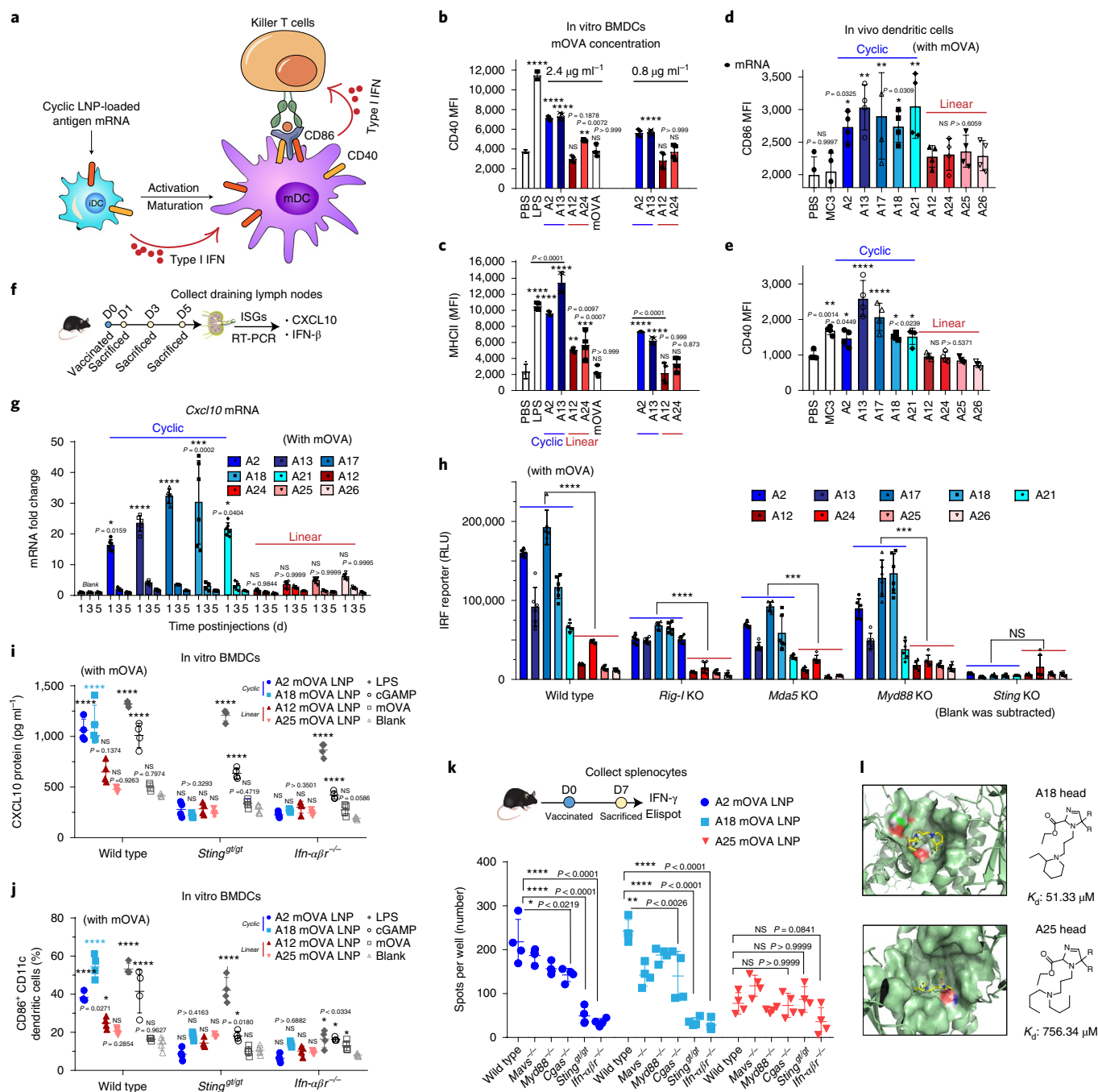


Fig. 5 | Cyclic lipidoids facilitate the maturation of APCs in local lymph nodes through STING-dependent activation of type I IFN. **a**, A schematic illustrating the process of APC activation and antigen presentation. **b–e**, FACS analysis of surface markers indicative of BMDC (**b,c**) and APC (**d,e**) maturation; cells isolated from local lymph nodes following treatment with cyclic LNPs ($n = 4$ biologically independent mice per group, $15 \mu\text{g mOVA}$ per mouse). **f,g**, mRNA expression levels of ISGs (interferon-stimulated genes; e.g., CXCL10) at local lymph nodes at 1, 3 and 5 d after vaccination, quantified using quantitative PCR ($n = 6$ biologically independent mice per group). **h**, IRF activation after incubating with LNPs ($0.1 \mu\text{g mOVA}$ per well) for 24 h in different CDS reporter cells (wild type or RIG-I, MDA5, MYD88 or STING KO) ($n = 4$ biologically independent experiments per group). **i**, CXCL10 protein levels measured by Bioplex ELISA in BMDCs (wild type, *Sting*^{gt/gt} and *Irf1*^{-/-}) treated with representative cyclic and linear mOVA LNPs ($1 \mu\text{g mOVA}$ RNA per well in a 12-well plate, $n = 4$ biologically independent mice per group). **j**, Percentage of CD86⁺ CD11c⁺ dendritic cells in BMDCs (wild type, *Sting*^{gt/gt} and *Irf1*^{-/-}) treated with representative cyclic and linear mOVA LNPs, measured by flow cytometry ($1 \mu\text{g mOVA}$ RNA per well in a 12-well plate, $n = 4$ biologically independent mice per group). **k**, ELISpot assay quantifications in different KO mouse groups ($15 \mu\text{g mOVA}$ per mouse, $n = 4$ biologically independent mice per group). **l**, Molecular docking of A25 and A18 with human STING. K_d values are calculated from the simulation. Data are presented as mean \pm s.d. Statistical significance was calculated by one-way ANOVA and Dunnett’s multiple comparisons test compared with untreated blank group: **** $P < 0.0001$, *** $P < 0.001$, ** $P < 0.01$, * $P < 0.05$. RLU, relative light units.

Activation of the STING pathway can occur indirectly through activating cGAS or through direct binding to STING proteins²⁰. Additional studies in *Cgas*^{-/-} mice showed that T-cell response was

only partially dependent on cGAS (Fig. 5k). We further evaluated the function of cGAS and STING in situ following vaccination with cyclic A18 LNPs. We observed elevation of phosphorylated IRF3

(pIRF3) in dendritic cells isolated from injection site and draining lymph nodes in wild-type and *Cgas*^{-/-} but not *Sting*^{tg/tg} mice, confirming that the activation of STING-type I IFN pathways could occur through cGAS-independent pathways (Supplementary Fig. 16). We also observed that cyclic LNPs interacted with both mouse and human STING pathways (Supplementary Fig. 17). We next performed several tests to determine whether our cyclic lipids can bind to human STING proteins. We used a lipid pull-down assay to assess binding between synthetic lipids and a His-tagged STING C-terminal domain (CTD). Extraction of His-tagged STING CTD after incubation with lipids suggested that, in contrast to linear lipid structures, cyclic lipids (notably A17 and A18) associate with STING protein (Supplementary Fig. 18a,b). In vitro, fluorescently labeled A18 cyclic LNPs were found within the endoplasmic reticulum (58.3% of LNPs) and colocalized with endoplasmic reticulum-associated STING protein (24.4% of LNPs) (Supplementary Fig. 18c). Using dynamic molecular docking, we next explored the interaction between lipid head groups and STING, and identified the STING CTD binding pocket (typically shared by the natural ligand c[G(2',5')pA(3',5')p]) (Protein Data Bank (PDB): 4EF4, 4KSY) and the small molecule DMXAA (PDB: 4QXP) as a likely binding site (Supplementary Fig. 18d,e). Simulations suggested that cyclic lipid head groups bind with ~3- to 20-fold greater affinity than their linear counterparts (cyclic A18, dissociation constant (K_d): 51.33 μ M; linear A25, K_d : 756.34 μ M; cyclic A2, K_d : 106.18 μ M; linear A12, K_d : 329.81, PDB: 4EF4) (Supplementary Fig. 18e).

Cyclic lipid-mRNA vaccines induce robust anti-tumor response.

We finally identified A18 (Fig. 6a) as our lead cyclic lipid candidate from our lipid library and screening tests. This lipid facilitates potent mRNA protein expression (Supplementary Figs. 11 and 19), and induces a strong immune response mediated, in part, through STING activation. We tested mRNA LNP formulations containing this cyclic lipid in a variety of tumor models. Using the B16-OVA melanoma model described earlier, we demonstrated that a single vaccination of A18 mOVA LNPs significantly prolonged survival, compared with either a PBS control group or mOVA vaccinations delivered using commercially available MC3 LNPs. Approximately 50% of animals treated with A18 LNPs survived over 40 d, and 3 of 11 animals were tumor free up to day 60 (Fig. 6b,c and Supplementary Fig. 20).

Next, we investigated vaccination with tyrosinase-related protein 2 (Trp2), a tumor-associated antigen known to be important in the B16F10 melanoma model⁵⁰. As both humans and mice share the same recognition sequence, this antigen has potential for clinical translation. Here, we delivered three doses of 15 μ g *Trp2* mRNA (mTRP2) in A18 or A25 LNPs, and compared this to free mLuc administered with the same dosing schedule, MC3 LNPs and protamine/mRNA complexes (representing the clinically investigated RNA active vaccine (CureVac))¹² (Fig. 6d,e and Supplementary Fig. 21a-c). A18, but not A25, LNPs were able to significantly slow tumor growth and outperformed all other delivery systems. Mice treated with the A18 mTRP2 LNPs showed a marked increase in

survival, with >60% living beyond 40 d. A18 LNP-vaccinated mice were further rechallenged with secondary B16F10 tumors at a distant site to the original tumors 1 d after vaccinations. Inhibition of secondary tumors has been observed, demonstrating that systemic and prolonged anti-tumor effects could be achieved through the administration of cyclic LNP-mediated mRNA vaccine (Supplementary Fig. 21d).

Next, we tested mRNA delivery in TC-1 cells expressing the human papillomavirus E7 protein, as a model for viral oncogene/mutant neo-epitope-driven cancer with translational vaccination potential¹¹. Vaccination using viral oncogene-coding E7 mRNA-A18 LNPs before day 5 significantly reduced tumor burden (Fig. 6f and Supplementary Fig. 20). When the A18 LNPs were co-administered with an anti-PD1 antibody therapy, animals demonstrated robust cures, even in late-stage treatment plans (Fig. 6g) (vaccination given from day 9 onwards; 30% mouse survival at 40 d (refs. ^{30,31})). Tumor tissue was collected from all three mouse models, and immunostaining indicated activated CD8⁺ T-cell infiltration in all models treated with A18 LNPs, confirming that these LNPs can induce a strong adaptive immune response (Fig. 6h-j).

Finally, we evaluated blood aspartate aminotransferase, alanine aminotransferase, blood urea nitrogen and creatine levels to determine whether repeated lipid injection caused systemic toxicity. We also compared major organs postvaccination using histology, and found no observable toxicity (Supplementary Figs. 22 and 23 and Supplementary Table 3). Moreover, selected LNPs were injected subcutaneously at a threefold higher dose than the vaccination dose. At 2, 8 and 24 h after injection, cytokine and chemokine concentrations were analyzed in systemic circulation and at the local injection site (24 h only) (Supplementary Fig. 24). In contrast to the PBS-treated group, both empty and mOVA-loaded A18 LNPs induced a pronounced release of pro-inflammatory cytokines (that is, tumor necrosis factor (TNF- α), IFN- γ and IL6) at the injection site. Importantly, the increase in cytokine concentrations following A18 LNPs vaccinations was predominantly local, with systemic cytokine levels much lower than in an LPS control. These data further demonstrate that these cyclic lipid systems can be used for safe and efficacious anti-tumor immunity.

Discussion

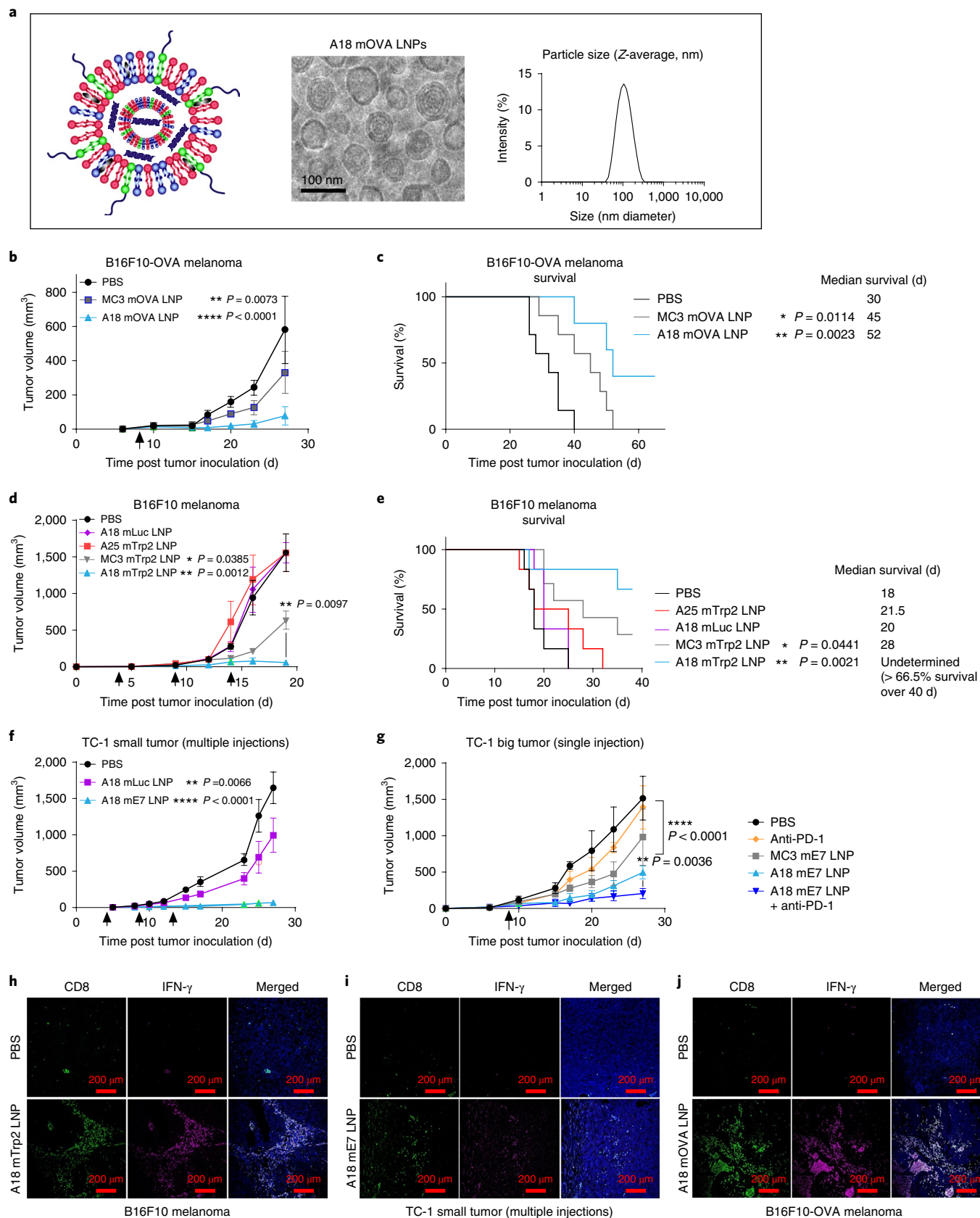
We have identified a class of cyclic lipids that provides robust anti-tumor efficacy through adjuvant-assisted mRNA vaccination in three mouse models. We rapidly synthesized a large lipid library containing over 1,000 compounds using a 3-CR in a single day. This reaction scheme expands classical multi-component reactions²⁷ by using an isocyanide-mediated three-component system, which allowed us to vastly increase the molecular diversity of our combinatorial library. Although multi-component reaction techniques have previously been used to generate molecular libraries^{27,51-53}, we provide evidence of an isocyanide-containing 3-CR lipid library for gene delivery. The addition of the isocyanide moiety allows the formation of a dihydroimidazole linker, and our results also provide

Fig. 6 | The effect of A18 mRNA antigen vaccines on tumor growth. **a**, Schematic, cryogenic electron microscopy image and particle size distribution of the finalized A18-mOVA-LNPs. **b-g**, Tumor inhibition and survival curves of three different types of tumor, B16F10-OVA ($n=7$ biologically independent mice per group per test) (**b,c**), B16F10 ($n=6$ biologically independent mice per group per test) (**d,e**) and TC-1 ($n=7$ biologically independent mice per group per test) (**f,g**), treated with different therapeutic mRNA vaccines alone, or together with anti-PD-1 antibody. PBS and A18 mOVA LNPs in all three models were repeated twice ($n=5$ biologically independent mice per group in the second repeat; individual mouse data presented in Supplementary Fig. 20) with similar results. Arrows indicate the dosing schedule; 15 μ g mRNA was dosed once or multiple times. Data are presented as mean \pm s.e.m. Two-way ANOVA combined with Tukey's multiple comparisons test was used to analyze the difference between different treatment groups. Unless stated otherwise, statistical analysis compared treatment groups and PBS controls. Survival curves were compared using log-rank (Mantel-Cox) test. In **c** and **f**, the statistical data on the chart compare A18 mTrp2 and A18 E7 mRNA + anti-PD-1 separately. * $P < 0.05$, ** $P < 0.01$, *** $P < 0.001$, **** $P < 0.0001$. **h-j**, Representative immunofluorescence staining of CD8/IFN- γ killer T cells within tumor regions of untreated or vaccine-treated mice. CD8 staining is shown as green; IFN- γ is shown as red; counterstain is DAPI (blue) in merged image shown at right ($n=5$ biologically independent mice per group).

an example of dihydroimidazole-containing LNPs for optimized mRNA delivery.

From this library, we identified nine lead candidate lipids that facilitated robust in vivo protein expression and antigen presentation

(Fig. 4a). Notably, lipids containing cyclic amino head groups (in particular, piperidiny six-member cyclic groups) were able to act as mRNA delivery vehicles but also facilitate APC maturation in an mRNA-independent manner (Fig. 5b). We demonstrated LNPs



with MYD88- and mRNA-independent, STING-mediated adjuvant effects. The STING pathway is emerging as an important regulator of innate immune cell behavior¹⁸, and activation of this pathway has been reported to correlate with reduced disease progression and better clinical outcomes in human cancer patients^{8–10}. Several small-molecule STING agonists are therefore currently in clinical trials^{10,54}; however, their success has been limited due to challenges with cytosolic delivery of these molecules²⁵.

In our system, the STING agonist is a lipid component of an LNP delivery system, which facilitates internalization. This combinatorial LNP intrinsically provides targeted adjuvant stimulation via the STING pathway and facilitates efficient mRNA delivery. We have used these materials to deliver antigen-specific mRNA vaccines in a number of in vivo tumor models, demonstrating significant survival advantage in animals treated with our lead candidate LNP A18. We envisage that these materials could be used as vaccine systems with a range of antigens, including tumor-associated antigens, personalized multi-epitope antigens and bacterial and viral proteins, and may provide a generalized approach towards vaccination.

Online content

Any methods, additional references, Nature Research reporting summaries, source data, statements of code and data availability and associated accession codes are available at <https://doi.org/10.1038/s41587-019-0247-3>.

Received: 15 August 2018; Accepted: 29 July 2019;

Published online: 30 September 2019

References

- Pardi, N., Hogan, M. J., Porter, F. W. & Weissman, D. mRNA vaccines—a new era in vaccinology. *Nat. Rev. Drug Discov.* **17**, 261–279 (2018).
- Pollard, C. et al. Type I IFN counteracts the induction of antigen-specific immune responses by lipid-based delivery of mRNA vaccines. *Mol. Ther.* **21**, 251–259 (2013).
- Jayaraman, M. et al. Maximizing the potency of siRNA lipid nanoparticles for hepatic gene silencing in vivo. *Angew. Chem. Int. Ed. Engl.* **51**, 8529–8533 (2012).
- Kauffman, K. J., Webber, M. J. & Anderson, D. G. Materials for non-viral intracellular delivery of messenger RNA therapeutics. *J. Control. Release* **240**, 227–234 (2016).
- Richner, J. M. et al. Modified mRNA vaccines protect against Zika virus infection. *Cell* **168**, 1114–1125.e10 (2017).
- Kariko, K. et al. Incorporation of pseudouridine into mRNA yields superior nonimmunogenic vector with increased translational capacity and biological stability. *Mol. Ther.* **16**, 1833–1840 (2008).
- Li, K., Qu, S., Chen, X., Wu, Q. & Shi, M. Promising targets for cancer immunotherapy: TLRs, RLRs, and STING-mediated innate immune pathways. *Int. J. Mol. Sci.* **18**, pii: E404 (2017).
- Zevini, A., OLAGNIE, D. & HISCO, J. Crosstalk between cytoplasmic RIG-I and STING sensing pathways. *Trends Immunol.* **38**, 194–205 (2017).
- Barber, G. N. STING: infection, inflammation and cancer. *Nat. Rev. Immunol.* **15**, 760–770 (2015).
- Corrales, L. et al. Direct activation of STING in the tumor microenvironment leads to potent and systemic tumor regression and immunity. *Cell Rep.* **11**, 1018–1030 (2015).
- Kranz, L. M. et al. Systemic RNA delivery to dendritic cells exploits antiviral defence for cancer immunotherapy. *Nature* **534**, 396–401 (2016).
- Fotin-Mlecsek, M. et al. Highly potent mRNA based cancer vaccines represent an attractive platform for combination therapies supporting an improved therapeutic effect. *J. Gene Med.* **14**, 428–439 (2012).
- Schlee, M. et al. Recognition of 5' triphosphate by RIG-I helicase requires short blunt double-stranded RNA as contained in panhandle of negative-strand virus. *Immunity* **31**, 25–34 (2009).
- Barbalat, R., Ewald, S. E., Mouchess, M. L. & Barton, G. M. Nucleic acid recognition by the innate immune system. *Annu. Rev. Immunol.* **29**, 185–214 (2011).
- Uchida, S. et al. Designing immunostimulatory double stranded messenger RNA with maintained translational activity through hybridization with poly A sequences for effective vaccination. *Biomaterials* **150**, 162–170 (2018).
- Van Lint, S. et al. Preclinical evaluation of TriMix and antigen mRNA-based antitumor therapy. *Cancer Res.* **72**, 1661–1671 (2012).
- Broos, K. et al. Particle-mediated intravenous delivery of antigen mRNA results in strong antigen-specific T-cell responses despite the induction of type I interferon. *Mol. Ther. Nucleic Acids* **5**, e326 (2016).
- Iurescia, S., Fioretti, D. & Rinaldi, M. Nucleic acid sensing machinery: targeting innate immune system for cancer therapy. *Recent Pat. Anticancer Drug Discov.* **13**, 2–17 (2018).
- Wang, J., Li, P. & Wu, M. X. Natural STING agonist as an “ideal” adjuvant for cutaneous vaccination. *J. Invest. Dermatol.* **136**, 2183–2191 (2016).
- Luo, M. et al. A STING-activating nanovaccine for cancer immunotherapy. *Nat. Nanotechnol.* **12**, 648–654 (2017).
- Caucheteux, S. M. & Piguat, V. New cutaneous vaccine adjuvant that STINGs a little less. *J. Invest. Dermatol.* **136**, 2127–2128 (2016).
- Iribarren, K. et al. Trial watch: immunostimulation with Toll-like receptor agonists in cancer therapy. *Oncoimmunology* **5**, e1088631 (2016).
- Holm, C. K. et al. Virus-cell fusion as a trigger of innate immunity dependent on the adaptor STING. *Nat. Immunol.* **13**, 737–743 (2012).
- Fu, J. et al. STING agonist formulated cancer vaccines can cure established tumors resistant to PD-1 blockade. *Sci. Transl. Med.* **7**, 283ra252 (2015).
- Wilson, D. R. et al. Biodegradable STING agonist nanoparticles for enhanced cancer immunotherapy. *Nanomedicine* **14**, 237–246 (2018).
- Demaria, O. et al. STING activation of tumor endothelial cells initiates spontaneous and therapeutic antitumor immunity. *Proc. Natl Acad. Sci. USA* **112**, 15408–15413 (2015).
- Hulme, C. & Gore, V. “Multi-component reactions: emerging chemistry in drug discovery” from xylocain to crixivan. *Curr. Med. Chem.* **10**, 51–80 (2003).
- Sahay, G. et al. Efficiency of siRNA delivery by lipid nanoparticles is limited by endocytic recycling. *Nat. Biotechnol.* **31**, 653–658 (2013).
- Gilleron, J. et al. Image-based analysis of lipid nanoparticle-mediated siRNA delivery, intracellular trafficking and endosomal escape. *Nat. Biotechnol.* **31**, 638–646 (2013).
- Cheng, N. et al. A nanoparticle-incorporated STING activator enhances antitumor immunity in PD-L1-insensitive models of triple-negative breast cancer. *JCI Insight* **3**, pii: 120638 (2018).
- Tanaka, Y., Hasui, T. & Sugimoto, M. Acid-free, aminoborane-mediated Ugi-type reaction leading to general utilization of secondary amines. *Org. Lett.* **9**, 4407–4410 (2007).
- Kazmaier, U. & Ackermann, S. A straightforward approach towards thiazoles and endothiopeptides via Ugi reaction. *Org. Biomol. Chem.* **3**, 3184–3187 (2005).
- Pan, S. C. & List, B. Catalytic three-component Ugi reaction. *Angew. Chem. Int. Ed. Engl.* **47**, 3622–3625 (2008).
- Fenton, O. S. et al. Bioinspired alkenyl amino alcohol ionizable lipid materials for highly potent in vivo mRNA delivery. *Adv. Mater.* **28**, 2939–2943 (2016).
- Akinc, A. et al. A combinatorial library of lipid-like materials for delivery of RNAi therapeutics. *Nat. Biotechnol.* **26**, 561–569 (2008).
- Koopmanschap, G., Ruijter, E. & Orru, R. V. Isocyanide-based multicomponent reactions towards cyclic constrained peptidomimetics. *Beilstein J. Org. Chem.* **10**, 544–598 (2014).
- Whitehead, K. A. et al. Degradable lipid nanoparticles with predictable in vivo siRNA delivery activity. *Nat. Commun.* **5**, 4277 (2014).
- Semple, S. C. et al. Rational design of cationic lipids for siRNA delivery. *Nat. Biotechnol.* **28**, 172–176 (2010).
- Kauffman, K. J. et al. Optimization of lipid nanoparticle formulations for mRNA delivery in vivo with fractional factorial and definitive screening designs. *Nano Lett.* **15**, 7300–7306 (2015).
- Whitehead, K. A. et al. In vitro-in vivo translation of lipid nanoparticles for hepatocellular siRNA delivery. *ACS Nano* **6**, 6922–6929 (2012).
- Chahal, J. S. et al. Dendrimer-RNA nanoparticles generate protective immunity against lethal Ebola, H1N1 influenza, and *Toxoplasma gondii* challenges with a single dose. *Proc. Natl Acad. Sci. USA* **113**, E4133–E4142 (2016).
- Sahin, U. et al. Personalized RNA mutanome vaccines mobilize poly-specific therapeutic immunity against cancer. *Nature* **547**, 222–226 (2017).
- Gu, B., Linehan, B. & Tseng, Y. C. Optimization of the buchi B-90 spray drying process using central composite design for preparation of solid dispersions. *Int. J. Pharm.* **491**, 208–217 (2015).
- Heyes, J., Palmer, L., Bremner, K. & MacLachlan, I. Cationic lipid saturation influences intracellular delivery of encapsulated nucleic acids. *J. Control. Release* **107**, 276–287 (2005).
- Oberli, M. A. et al. Lipid nanoparticle assisted mRNA delivery for potent cancer immunotherapy. *Nano Lett.* **17**, 1326–1335 (2017).
- Kuai, R., Ochyl, L. J., Bahjat, K. S., Schwendeman, A. & Moon, J. J. Designer vaccine nanodiscs for personalized cancer immunotherapy. *Nat. Mater.* **16**, 489–496 (2017).
- Ma, D. Y. & Clark, E. A. The role of CD40 and CD154/CD40L in dendritic cells. *Semin. Immunol.* **21**, 265–272 (2009).
- Walseng, E. et al. Dendritic cell activation prevents MHC class II ubiquitination and promotes MHC class II survival regardless of the activation stimulus. *J. Biol. Chem.* **285**, 41749–41754 (2010).

49. Deering, R. P., Kommareddy, S., Ulmer, J. B., Brito, L. A. & Geall, A. J. Nucleic acid vaccines: prospects for non-viral delivery of mRNA vaccines. *Expert Opin. Drug Deliv.* **11**, 885–899 (2014).
50. Bloom, M. B. et al. Identification of tyrosinase-related protein 2 as a tumor rejection antigen for the B16 melanoma. *J. Exp. Med.* **185**, 453–459 (1997).
51. Aviles, E. et al. Synthesis and preliminary biological evaluation of a small library of hybrid compounds based on Ugi isocyanide multicomponent reactions with a marine natural product scaffold. *Bioorg. Med. Chem. Lett.* **25**, 5339–5343 (2015).
52. Ugi, I., Werner, B. & Dömling, A. The chemistry of isocyanides, their multicomponent reactions and their libraries. *Molecules* **8**, 4 (2003).
53. Wada, J. et al. A new nonsteroidal antiinflammatory agent. 2-Substituted 5- or 6-benzothiazoleacetic acids and their derivatives. *J. Med. Chem.* **16**, 930–934 (1973).
54. Ohkuri, T. et al. Intratumoral administration of cGAMP transiently accumulates potent macrophages for anti-tumor immunity at a mouse tumor site. *Cancer Immunol. Immunother.* **66**, 705–716 (2017).

Acknowledgements

This work was supported by Translate Bio (Lexington, MA) and the Juvenile Diabetes Research Foundation (grant nos. 17-2007-1063 and 3-PDF-2015-91-A-N). This work is supported in part by the Cancer Center Support (core) (grant no. P30-CA14051) from the National Institutes of Health. D.G.A. is a consultant for Translate Bio. L.M. was supported by a Misrock postdoctoral fellowship. D.D. was supported by an EPSRC E-TERM Fellowship (EP/I017801/1) and a Marie Skłodowska Curie Fellowship (IF/798348). K.S. was supported by the Ruth L. Kirschstein NRSA Postdoctoral Fellowship (no. 1F32EB025688-01A1) from the National Institute of Biomedical Imaging and Bioengineering of the National Institutes of Health. L.L. and J.H. were supported by a Ming Wai Lau grant from the Ming Wai Lau Centre for Reparative Medicine, Karolinska Institutet. The authors would like to acknowledge the use of resources at the W. M. Keck Biological Imaging Facility (Whitehead Institute) and at the Microscopy, Histology, Animal Imaging & Preclinical Testing and Flow Cytometry Core Facilities (Swanson Biotechnology Center, David H. Koch Institute for Integrative Cancer Research at MIT), and acknowledge Wuxi Further Pharmaceutical Co., Ltd for synthesizing and providing lipid materials.

Author contributions

L.M. and D.G.A. designed experiments and analyzed data. L.L. designed the chemical structures. L.M., Y.H., D.D., Y.S., J.C., K.S., W.G. and J.H. performed experiments. J.L. and L.M. drew the schematic figures. L.M., D.D., J.C.D., Y.H. and D.G.A. wrote the manuscript. R.L. and D.G.A. supervised the study. All authors discussed the results and assisted in the preparation of the manuscript.

Competing interests

L.M., Y.H., L.L. and D.G.A. have filed a patent for the development of the described lipids synthesized using the three-component reaction. R.L. receives licensing fees (to patents in which he was an inventor on) from, invested in, consults (or was on scientific advisory boards or boards of directors) for, lectured (and received a fee), or conducts sponsored research at MIT for which he was not paid for the following entities: 7th Sense, Abpro, Aleph Farms, Alkermes, Allevi, Alnylam, Artificial Cells, Arsenal Medical, BASF, Celero, Cellomics, Cellular Biomedical, Clarus, Clontech, Combined Therapeutics, Conference Forum, Curis, Domain, Eagle, Echo, Edge, Evox, Fate Therapeutics, Frequency Therapeutics, Genscript, Glycobia, Glympse, Grandhope, Greenlight, HKF Technologies, Horizon Discovery, Humacyte, Indivior, Inovio, Institute of Immunology, In Vivo Therapeutics, Ironwood Pharmaceuticals, Kallyope, Kensa, Keratinx, KSQ Therapeutics, Laderatech, Inc., Landsdowne Labs, Like Minds, Luminopia, Luye, Lyndra, Lyra, Medical Kinetics, Merck, Micelle, Moderna, Momenta, Monsanto, Mylan, Nanobiosym, Nanobiotix, Noveome, Particles for Humanity, Perosphere, Pfizer, Polaris, Portal, Pulmatrix, Puretech, Roche, Rubius, Secant, Selecta Biosciences, Setsuro, Shiseido, Sigilon, Sio2, SQZ, Stembiosys, Suono Bio, T2 Biosystems, Tara, Taris Biomedical, Tarveda, Third Rock, Tiba, Tissium, Titan Pharma, Unilever, VasoRX, Verseau Therapeutics, Vivtex, Wiki Foods and Zenomic.

Additional information

Supplementary information is available for this paper at <https://doi.org/10.1038/s41587-019-0247-3>.

Correspondence and requests for materials should be addressed to D.G.A.

Reprints and permissions information is available at www.nature.com/reprints.

Publisher's note Springer Nature remains neutral with regard to jurisdictional claims in published maps and institutional affiliations.

© The Author(s), under exclusive licence to Springer Nature America, Inc. 2019

Methods

Material and lipid library synthesis. Lipids were synthesized through one-pot mixing of amines, ketones and isocyanides. Amines were purchased from Sigma-Aldrich, TCI America and Alfa Aesar. All isocyanides were purchased from Sigma-Aldrich. Ketones were mainly purchased from Sigma-Aldrich, Alfa Aesar and TCI America. All chemicals obtained from commercial sources were used as received. The lipid was synthesized with a molar ratio of amine/isocyanide/ketone of 1:1:1. All library reactions were carried out in 96-well deep-well plates with glass inserts (VWR). The reactions took place at room temperature for 24 h; conversion was typically over 70%. For in vitro high-throughput transfection study or in vivo batch analysis assay, the lipid mixtures were used without purification. Otherwise, the lipid was purified by flash column chromatography on an Isco Combiflash system. Structure was confirmed by ^1H and ^{13}C NMR spectrometry (Bruker AVANCE-400 NMR spectrometer with a Magnex Scientific superconducting magnet) and liquid chromatography–mass spectrometry (LC-MS) (Waters Acquity LC-MS instrument) (see Supplementary Notes for details).

LNP synthesis. An organic phase was prepared by solubilizing with ethanol a mixture of the synthesized cationic lipid, DOPE (Avanti), cholesterol (Avanti) and C14-PEG 2000 (Avanti) at a predetermined molar ratio. The aqueous phase was prepared in 10 mM citrate buffer (pH 3.0, Fisher) with mLuc (firefly mLuc, Translate), antigen mRNA or nontranslating Cy5-labeled Fluc mRNA (TriLink BioTechnologies). All mRNAs were stored at -80°C , and were allowed to thaw on ice before use. The ethanol and aqueous phases were mixed at a 3:1 ratio and a lipid/mRNA weight ratio of 10:1 in a microfluidic chip device using syringe pumps as previously described³⁹. Resultant LNPs were dialyzed against 1X PBS in a 20,000 MWCO cassette (Fisher) at 4°C for 1 h and were stored at 4°C before injection. For high-throughput screening, the LNPs were prepared in a 96-well plate by directly adding ethanol phase to aqueous phase. For in vitro screening, LNPs were directly incubated with cells without further dialysis. For in vivo batch analysis screening, LNPs in each classification group (for batch analysis) were mixed and dialyzed against 1X PBS before injection into mice.

LNP formulation optimization. The molar ratio among different lipid components and the weight ratio between mRNA and total lipid would affect the encapsulation, morphology and transfection efficiency of LNPs³⁹; thus, these factors were optimized using four-factor (DOPE, C14-PEG, cationic lipid, mRNA/lipid ratio), four-level central composite design. The experiments were designed and analyzed using Design-Expert software version 11 (Stat-Ease)^{43,55,56}.

LNP characterization. The size, polydispersity index and zeta potentials of LNPs were measured using dynamic light scattering (ZetaPALS, Brookhaven Instruments). Diameters are reported as the intensity mean peak average. To calculate the nucleic acid encapsulation efficiency, a modified Quant-iT RiboGreen RNA assay (Invitrogen) was used as previously described^{39,45}. Results of encapsulation efficiency can be found in Supplementary Table 3.

RNA synthesis. RNAs from studies of firefly-luciferase and OVA expression in tissue culture and in vivo were obtained from Translate Bio and TriLink^{39,41,45}. E7 mRNA was generated from linearized plasmid vectors by in vitro transcription using MEGAscript kits (Life Technologies), 5' capped to produce cap-0 structured 7-methylguanylate 5' ends using ScriptCap m7G Capping System kits (CellScript) and 3' poly(A)-tailed using A-Plus Poly(A) Polymerase Tailing kits (CellScript), all according to the manufacturers' protocols.

In vitro high-throughput screening and in vivo batch analysis. The unpurified lipid library was directly added to ethanol containing DOPE, cholesterol and C14-PEG at a predetermined molar ratio, and then mixed with mLuc aqueous solution. For in vitro transfection, the lipid-mRNA mixture (with 0.1 μg mRNA was added to 96-well plates preseeded with HeLa cells, BMDCs or BMDMs. After overnight incubation, the mLuc transfection efficiency and the cell viability were simultaneously measured using ONE-Glo Luciferase Assay System (Promega) according to manufacturer's instructions. The fluorescence and luminescence were quantified using Tecan Infinite M200 Pro plate reader (Tecan). For the in vivo batch analysis assay, lipid-mRNA mixtures within one classification group were mixed and dialyzed before injection into mice. Then, 50 μg (~ 2.5 mg kg^{-1}) mLuc RNA for batch analysis 1 (120 LNP mixtures in each group), 15 μg (~ 0.75 mg kg^{-1}) mLuc RNA per mouse for batch analysis 2 (12 LNP mixtures in each group) and 10 μg (~ 0.5 mg kg^{-1}) for batch analysis 3 were injected for each lipid group. At 5 h after injection, mice were subjected to the bioluminescence assay using an in vivo imaging system (IVIS kinetic imaging system, Perkin Elmer).

Animals and cells. All animal procedures were performed with ethical compliance and approval by the Massachusetts Institute of Technology Committee on Animal Care. Female C57BL/6 mice (4–8 weeks) were obtained from the Jackson Laboratory and Charles River Laboratories. *Ifn- $\alpha\beta$* ^{-/-}, *Mavs*^{-/-}, *Sting*^{elst}, *Myd88*^{-/-} and Ai14D (B6.Cg-*Gt(ROSA)26Sor*^{tm14(CAG-tdTomato)Hze/J}, 007914) mice were purchased from the Jackson Laboratory and housed in an Massachusetts Institute of Technology animal facility. For each experiment, mice were randomly

allocated by blinded investigators to each group. *Sting*^{elst} and *Ifn- $\alpha\beta$* ^{-/-} BMDCs were derived from corresponding KO mice and then cultured in granulocyte-macrophage colony-stimulating factor (GM-CSF)-containing medium for 6–7 d. CDS reporter cells, including RAW-Lucia ISG cells (for example, wild type, KO-*Sting*, KO-*Rig-I*, KO-*Mda5*) and THP1-Dual cells (for example, wild type, KO-*MYD* cells, KO-*STING* cells THP1) were purchased from InvivoGen. The B16-OVA cell line was kindly given by Dr. Kenneth Rock, Dana-Farber Cancer Institute, Boston. TC-1 cells were kindly provided by the Darrell Irvine laboratory (Massachusetts Institute of Technology). B16F10 cells and HeLa cells were purchased from ATCC. All cell lines were routinely tested using a mycoplasma contamination kit (R&D Systems). B16F10, B16-OVA, HeLa and TC-1 cells were cultured in complete medium (RPMI 1640, 10% fetal bovine serum, Pen-Strep (100 U ml⁻¹ and 100 $\mu\text{g ml}^{-1}$, respectively)). CDS reporter cells were cultured with RPMI1640, 10% fetal bovine system supplemented with 100 $\mu\text{g ml}^{-1}$ Normocin (Invitrogen), 2 mM L-glutamine (Invitrogen), 25 mM HEPES (Invitrogen) at 37°C in 5% CO₂.

Bioluminescence. At 5, 6, 24 and 48 h (or longer) after the injection of the mRNA LNPs, mice were injected intraperitoneally with 0.2 ml D-luciferin (10 mg ml^{-1} in PBS). The mice were anesthetized in a ventilated anesthesia chamber with 1.5% isoflurane in oxygen and imaged 10 min after the injection with an in vivo imaging system (IVIS, PerkinElmer). Luminescence was quantified using the Living Image software (PerkinElmer)³⁹.

Ai14D reporter mice transfection analysis. Ai14D mice were immunized with A2 and A12 LNPs containing mRNA coding for either Cre-recombinase or irrelevant mRNA, with 0.5 mg kg^{-1} mRNA per mouse (TriLink). At 2 d after vaccination, the draining lymph nodes, the inguinal lymph nodes, were removed and digested in a medium containing collagenase D (1 mg ml^{-1} , Sigma) for 40 min at 37°C . The solution was then filtered through a 70 μm cell strainer and centrifuged. The cells were suspended at 4°C in staining buffer for 30 min at 4°C . The staining buffer contained antibodies specific for different cell markers and analyzed by flow cytometry.

In vivo cytotoxic T lymphocyte (CTL) assay. Groups of C57BL/6 mice were injected with 15 μg naked or LNP-loaded mOVA and mLuc control, OVA peptide, or OVA protein with other adjuvant (LPS or cGAMP (InvivoGen)) subcutaneously in the lower left flank. At 5 d after the second injection, naive C57BL/6 mice were killed and splenocytes were dissociated and collected. Half of the splenocytes were pulsed with OVA_{257–265} or E7_{49–57} peptides (InvivoGen) in complete medium at 37°C for 2 h. The unpulsed and peptide-pulsed cells were labeled with 0.05 μM or 0.5 μM carboxyfluorescein succinimidyl ester (CFSE) (Invitrogen), respectively, in PBS for 20 min. After washing of the CFSE, equal numbers (1×10^7) of CFSE_{low} (unpulsed) and CFSE_{high} (peptide-pulsed) cells were mixed together and instantly injected intravenously into the immunized mice. At 18 h after injection, splenocytes and lymph nodes from the treated mice were collected, dissociated and subjected to flow cytometry analysis. The numbers of CFSE_{high} and CFSE_{low} cells were confirmed and used to calculate the percentage of peptide-pulsed target cell killing. Specific killing was defined as: percentage of specific lysis = $(1 - \text{nontransferred control ratio/experimental ratio}) \times 100$ (ref. 20).

ELISpot assay. Multiscreen filter plates (R&D Systems), precoated with antibodies specific for IFN- γ (R&D Systems), were washed with PBS and blocked with full medium for 3 h. Then, 2×10^5 effector cells (splenocytes, purified CD4⁺ T cells or purified CD8⁺ T cells (using untouched CD8 α T cells or CD4 α T cells isolation kit II (Miltenyi Biotec)) per well were stimulated for 16–20 h with 2 $\mu\text{g ml}^{-1}$ OVA or E7 peptide or autologous dendritic cells loaded with RNA or loaded with peptides. All tests were performed in duplicate or triplicate and included assay positive controls as well as cells from a reference donor with known reactivity. Spots were visualized with a biotin-conjugated anti-IFN- γ antibody (R&D Systems) followed by incubation with ExtrAvidin-Alkaline Phosphatase (R&D Systems) and BCIP/NBT substrate (R&D Systems). Plates were scanned using CTL ImmunoSpot Series S five Versa ELISpot Analyzer (S5Versa-02-9038) and analyzed by ImmunoCapture v.6.3 software^{22,57}.

Enzyme-linked immunosorbent assay (ELISA). For antibody detection, groups of C57BL/6 mice were immunized with different vaccines on days 0 and 5. On days 7, 10 and 14, 100 μl blood was drawn from the tail vein, and levels of antigen-specific IgG in the serum were measured by ELISA. For ELISA, flat-bottomed 96-well plates (Nunc) were precoated with OVA protein at a concentration of 2 μg protein per well in 100 mM carbonate buffer (pH 9.6) at 4°C overnight, which were then blocked with 10% fetal bovine serum (FBS) in PBS-Tween (PBS-T). Antisera obtained from immunized animals were diluted 50 times in PBS-T (PBS-0.05% Tween), pH 7.4, and were added to the wells and incubated at 37°C for 2 h. Horseradish peroxidase-conjugated goat anti-mouse IgG (no. 7076, Cell Signaling) was used at a dilution of 1:5,000 in PBS-T-10% FBS for labeling. After adding the horseradish peroxidase substrates, optical densities were determined at a wavelength of 450 nm in an ELISA plate reader (Bio-Rad)^{20,41,45}.

BMDC activation and antigen presentation assay. BMDCs were prepared as described previously^{20,46}. In brief, bone marrow cells flushed from the femurs of C57BL/6J mice were cultured in the dendritic cell medium: RPMI 1640 supplemented with 10% FBS, Pen-Strep and 20 ng ml⁻¹ GM-CSF. The medium was half replaced every 2 d. On day 6, nonadherent and loosely adherence immature dendritic cells were collected and plated at 5 × 10⁵ cells per well in a 24-well plate. The phenotypes of dendritic cells were predetermined using CD11c (routinely 60–80% CD11c⁺). After 24 h, BMDCs were incubated with ~0.5–2.5 μg mOVA in various LNPs formulations or with blank LNPs at the same dosage in complete medium for different lengths of time (10 h, 24 h, 48 h) at 37 °C with 5% CO₂; LPS was used as a dendritic cell activation positive control. After co-incubation, BMDCs were collected, washed with FACS buffer (1% BSA, 10% FBS in PBS), incubated with anti-CD16/32 at room temperature and then stained on ice with fluorophore-labeled antibodies against CD45, CD11c, CD40, CD86, F4/80, MHCII or PE-conjugated anti-mouse SIINFEKL/H-2Kb monoclonal antibody 24-D1.16 (eBioscience). The activation of dendritic cells and antigen presentation were quantified using the mean fluorescence intensity of cells by flow cytometry analysis.

Flow cytometry and antibodies. Antibodies purchased from BioLegend, eBioscience and BD for flow cytometry are listed in Supplementary Table 4. For the flow cytometry analysis of surface markers, cells were pre-incubated with anti-CD16/32 antibody and stained on ice with fluorophore-conjugated antibody. For the staining of intracellular markers, for example, IFN-γ, cells were prestimulated with the Cell Stimulation Cocktail (eBioscience) for 6 h, and fixed and permeabilized using the fixation/permeabilization solution kit (BD). Then, cells were stained with anti-IFN-γ or other surface antibodies. Flow data were acquired on a BD LSR II flow cytometer and analyzed using FlowJo software.

Quantitative PCR with reverse transcription (RT-qPCR). Local lymph nodes and tumors were taken at indicated time points after injection with LNPs loaded mRNA antigen. For the in vitro study, BMDCs were cultured and treated as mentioned above. Total RNAs were extracted by RNeasy Kit (Qiagen) from cells or tissues according to manufacturer's instructions. cDNA was generated using SuperScript III First-Strand Synthesis System (Invitrogen). RT-qPCR was performed according to the TaqMan Gene Expression Assay protocols (Invitrogen) using a 384-well LightCycler 480 (Roche)^{20,58}. Samples were run in triplicate. The following primers were used for RT-qPCR: *Cxcl10* (mouse, Mm00445235_m1, Invitrogen), *Ifnb1* (mouse, Mm00439552_s1, Invitrogen), *Irf7* (mouse, Mm00516793_g1, Invitrogen), *Gapdh* (mouse, Mm99999915_g1, Invitrogen), *CXCL10* (human, Hs00171042_m1, Invitrogen), *IFNB1* (human, Hs01077958_s1, Invitrogen) and *GAPDH* (human, Hs02786624_g1).

STING pulldown assay. To investigate the STING interaction with cyclic lipid, we prepared and purified His-Sting CTD according to a previous method²⁰. The His-STING was bound to Ni-NTA followed by co-incubation with lipids for 1 h at room temperature. The extra lipids were washed four times with cold PBS. Lipid bonded to protein was finally extracted using propanol and quantified using ultraperformance liquid chromatography–mass spectrometry (UPLC-MS, Waters).

Immunization and tumor therapy experiments. Mice aged 4–6 weeks were injected subcutaneously with B16-OVA or B16F10 melanoma cells (1.5 × 10⁵) or TC-1 cells (1.5 × 10⁵) into the right flank. Vaccination timelines were selected based on the growth curves of the mouse models and according to literature descriptions^{20,45}. In most cases, vaccinations began when tumor sizes was less than 50 mm³ (on day 4 or 5 after tumor inoculation). Animals were immunized by subcutaneous injection of different LNP formulations containing 15 μg mOVA,

mLuc, E7 mRNA or mTrp2, as described in the main text. Two (B16-OVA tumors) or three doses (B16F10 and TC-1 tumors) were given every 5 d. Alternatively, a single dose of vaccination was given at a larger tumor size for B16-OVA and TC-1 tumor models (on day 9 after tumor inoculation) to further confirm the potent anti-tumor efficacy of our LNPs. For combinatorial immunotherapy, at days 5, 8, 11 and 14 after inoculation, some groups were intraperitoneally injected with 200 μg checkpoint inhibitor (anti-mPD-1, BioXcell or BE0146). Tumor growth was measured three times a week using a digital caliper and calculated as 0.5 × length × width^{2,20,46}. Mice were euthanized when the tumor volumes reached 2,000 mm³. For the lung metastasis rechallenge model, tumor-bearing vaccinated or nonvaccinated mice were rechallenged by intravenous injection of 5 × 10⁴ B16-OVA cells per mouse, and lungs were excised on day 21. For the subcutaneous rechallenge model, 1 d after second vaccination (two vaccinations in total), mice bearing A18 LNP-treated melanoma were rechallenged with B16F10 cells (1.5 × 10⁵) on their distant side. Tumor inhibition was compared with mice bearing freshly inoculated tumors (no previous challenge).

Hematoxylin and eosin morphology evaluation and blood chemistry analysis. At 3 d after second vaccination, tumor-free and tumor-bearing mice with different treatments were all subjected to a toxicity assay. Creatinine, total bilirubin, blood urea nitrogen, and serum aspartate aminotransferase and alanine aminotransferase were assayed as indicators of renal and liver function, respectively. Major organs, including the heart, liver, spleen, lungs and kidneys, were collected and fixed for hematoxylin and eosin staining by the KI Swanson Biotechnology Center to evaluate the organ-specific toxicity.

Statistical analysis. A two-tailed Student's *t*-test or a one-way analysis of variance (ANOVA) was performed when comparing two groups or more than two groups, respectively. Statistical analysis was performed using Microsoft Excel and Prism 7.0 (GraphPad). Data are expressed as means ± s.d. Difference was considered to be significant if *P* < 0.05 (**P* < 0.05, ***P* < 0.01, ****P* < 0.001, *****P* < 0.0001 unless otherwise indicated). The survival rates of the two groups were analyzed using a log-rank test and were considered statistically significant if *P* < 0.05.

Reporting Summary. Further information on research design is available in the Nature Research Reporting Summary linked to this article.

Data availability

The data supporting the findings of this study are available from the corresponding author upon reasonable request.

References

- Rao, R. S., Kumar, C. G., Prakasham, R. S. & Hobbs, P. J. The Taguchi methodology as a statistical tool for biotechnological applications: a critical appraisal. *Biotechnol. J.* **3**, 510–523 (2008).
- Belliveau, N. M. et al. Microfluidic synthesis of highly potent limit-size lipid nanoparticles for in vivo delivery of siRNA. *Mol. Ther. Nucleic Acids* **1**, e37 (2012).
- Feig, C. et al. Targeting CXCL12 from FAP-expressing carcinoma-associated fibroblasts synergizes with anti-PD-L1 immunotherapy in pancreatic cancer. *Proc. Natl. Acad. Sci. USA* **110**, 20212–20217 (2013).
- Maruggi, G. et al. Immunogenicity and protective efficacy induced by self-amplifying mRNA vaccines encoding bacterial antigens. *Vaccine* **35**, 361–368 (2017).

Reporting Summary

Nature Research wishes to improve the reproducibility of the work that we publish. This form provides structure for consistency and transparency in reporting. For further information on Nature Research policies, see [Authors & Referees](#) and the [Editorial Policy Checklist](#).

Statistics

For all statistical analyses, confirm that the following items are present in the figure legend, table legend, main text, or Methods section.

n/a Confirmed

- The exact sample size (n) for each experimental group/condition, given as a discrete number and unit of measurement
- A statement on whether measurements were taken from distinct samples or whether the same sample was measured repeatedly
- The statistical test(s) used AND whether they are one- or two-sided
Only common tests should be described solely by name; describe more complex techniques in the Methods section.
- A description of all covariates tested
- A description of any assumptions or corrections, such as tests of normality and adjustment for multiple comparisons
- A full description of the statistical parameters including central tendency (e.g. means) or other basic estimates (e.g. regression coefficient) AND variation (e.g. standard deviation) or associated estimates of uncertainty (e.g. confidence intervals)
- For null hypothesis testing, the test statistic (e.g. F , t , r) with confidence intervals, effect sizes, degrees of freedom and P value noted
Give P values as exact values whenever suitable.
- For Bayesian analysis, information on the choice of priors and Markov chain Monte Carlo settings
- For hierarchical and complex designs, identification of the appropriate level for tests and full reporting of outcomes
- Estimates of effect sizes (e.g. Cohen's d , Pearson's r), indicating how they were calculated

Our web collection on [statistics for biologists](#) contains articles on many of the points above.

Software and code

Policy information about [availability of computer code](#)

Data collection

FACS DIVA, Living Image v 4.5.5, CTL ImmunoSpot Series S five Versa ELISpot Analyzer (S5Versa-02-9038)

Data analysis

Graphpad Prism v8, FlowJo v10, Chemdraw v17.1, ImageJ, ImageScope, Living Image v 4.5.5, Design Expert 11, CTL ImmunoSpot Series S five Versa ELISpot Analyzer (S5Versa-02-9038), AutoDock 4.2

For manuscripts utilizing custom algorithms or software that are central to the research but not yet described in published literature, software must be made available to editors/reviewers. We strongly encourage code deposition in a community repository (e.g. GitHub). See the Nature Research [guidelines for submitting code & software](#) for further information.

Data

Policy information about [availability of data](#)

All manuscripts must include a [data availability statement](#). This statement should provide the following information, where applicable:

- Accession codes, unique identifiers, or web links for publicly available datasets
- A list of figures that have associated raw data
- A description of any restrictions on data availability

All data generated during this study are included in this published article (and its supplementary information files).

Field-specific reporting

Please select the one below that is the best fit for your research. If you are not sure, read the appropriate sections before making your selection.

- Life sciences Behavioural & social sciences Ecological, evolutionary & environmental sciences

Life sciences study design

All studies must disclose on these points even when the disclosure is negative.

Sample size	No sample size calculation was performed. Instead, we relied on journal guidelines for a minimum of n = 4 for in vitro and some in vivo tests. For anti-tumor efficacy and immunology assay, minimum of n=6 animals/treatment group, except with the initial high throughput screening, n=2 were used due to large sample size. Numbers in this case are also clearly reported in the Figure Legend. In addition, we adhered to sample size requirements necessary for determining statistical significance.
Data exclusions	Some cyclic and linear lipids in the second library with very low mRNA delivery efficiency were excluded. Lipid candidates with mRNA delivery efficiency relevant to KC3 and MC3 lipids were recorded.
Replication	All attempts at replication were successful. Experimental repeat numbers are also reported in Figure Legends.
Randomization	Animal groups were randomized by body weight and/or age.
Blinding	Experiments were generally blinded.

Reporting for specific materials, systems and methods

We require information from authors about some types of materials, experimental systems and methods used in many studies. Here, indicate whether each material, system or method listed is relevant to your study. If you are not sure if a list item applies to your research, read the appropriate section before selecting a response.

Materials & experimental systems

n/a	Involved in the study
<input type="checkbox"/>	<input checked="" type="checkbox"/> Antibodies
<input type="checkbox"/>	<input checked="" type="checkbox"/> Eukaryotic cell lines
<input checked="" type="checkbox"/>	<input type="checkbox"/> Palaeontology
<input type="checkbox"/>	<input checked="" type="checkbox"/> Animals and other organisms
<input checked="" type="checkbox"/>	<input type="checkbox"/> Human research participants
<input checked="" type="checkbox"/>	<input type="checkbox"/> Clinical data

Methods

n/a	Involved in the study
<input checked="" type="checkbox"/>	<input type="checkbox"/> ChIP-seq
<input type="checkbox"/>	<input checked="" type="checkbox"/> Flow cytometry
<input checked="" type="checkbox"/>	<input type="checkbox"/> MRI-based neuroimaging

Antibodies

Antibodies used	All the antibodies (name, vendor, catalog, dilution factors) were provided in the method section (under "flow cytometry and antibodies" section). CD-11b-APC, M1/70, anti-mouse, eBioscience, 17-0112-82, 1/800 dilution; CD11c-PE-Cy7, N418, anti-mouse, eBioscience, 25-0114-82, 1/800 dilution; Ly-6G/Ly-6C-FITC, RB6-8C5, anti-mouse, eBioscience, 11-5931-81, 1/200 dilution; Ly-6G/Ly-6C-PE, RB6-8C5, anti-mouse, eBioscience, 12-5931-81, 1/200 dilution; MHCII-APC-Cy7, I-A/I-E, anti-mouse, 47-5321-82, 1/200 dilution; CD8a-Alexa 700, 53-6.7, anti-mouse, eBioscience, 1/400 dilution; CD4-PerCP-Cy5.5, RM4-5, BD, 550954, 1/400 dilution; CD4-FITC, RM4-5, anti-mouse, BD, 553046, 1/400 dilution; CD45R/B220-APC, RA3-6B2, BD, 561880, 1/800 dilution; CD45.2-V500, 104, anti-mouse, BD, 562129, 1/200 dilution; F4/80 FITC, EMR1, anti-mouse, BioLegend, 123107, 1/400 dilution; NK1.1-APC-Cy7, PK136, BD, 560618, 1/400 dilution; CD3-APC, 17A2, anti-mouse, eBioscience, 50-148-40, 1/400 dilution; CD16/32, Biolegend, 101320, 1/50 dilution; 25-D1.16-PE, Biolegend, 141603, 1/200 dilution; CD86-pacific blue, GL-1, anti-mouse, 105022, BioLegend, 1/400 dilution; CD40-PE-Cy7, 3/23, anti-mouse, BioLegend, 124621, 1/400; IFN-gamma-PE, XMG 1.2 (RUO), anti-mouse, 562020, BD, 1/200 dilution; HRP conjugated goat anti-mouse IgG, 7076, cell signaling, 1/5000 dilution;
Validation	All primary antibodies were bought from vendors (BD, biolegend, ebioscience, abcam), used for the species suggested by the manufacturers (mouse-specific). Validations can be found in the manufacturer's website. In addition, many have literature references and species specifications on their websites. CD4, CD8, CD45.2, B220, B19, NK 1.1, CD3, CD11b+ et al. are routinely used antibodies. Dilution factors were pre-determined in the lab. Flow data suggests clear isolation of the cell populations (Fig. S6). IFN-gamma-PE dilution factor was suggested in the manufacturer's website (http://wwwbdbiosciences.com/ds/pm/tds/562020.pdf), and further confirmed by us using titration assay (FACS).

Eukaryotic cell lines

Policy information about [cell lines](#)

Cell line source(s)	Cell line sources were provided under "Method: animal and cell" section. Most of them are from ATCC, InvivoGen, or from collaborators. Sting gt/gt, and Ifn- α /Br-/- BMDCs were derived from corresponding knockout mice and then cultured in GM-CSF-containing medium for 6–7 days. CDS reporter cells, including RAW-Lucia TM ISG cells (e.g., wild type, KO-Sting, KO-Rig-I, KO-Mda5) and THP1-DualTM (e.g., wild type, KO-MYD cells, KO-STING cells) were purchased from InvivoGen Inc. (CA). B16-
---------------------	--

Authentication	OVA cell line was kindly given by Dr. Kenneth Rock, Dana-Farber Cancer Institute, Boston. TC-1 cells were kindly provided by Darrell Irvine lab (MIT). B16-F10 cells and HeLa cells were purchased from ATCC.
Authentication	The cell lines were certified by the manufacturers (surface markers, morphology). Knockout cell lines were verified using positive or negative controls according to manufacturers' suggestions and compared with the data provided by manufacturers. TC-1 and OVA cell lines were verified by their sensitivity to OVA peptide and E7 peptide using IFN-gamma Elispot Assay.
Mycoplasma contamination	Cell lines were all tested negative for mycoplasma contamination (Lonza MycoAlert kit).
Commonly misidentified lines (See ICLAC register)	N/A. This is not a problem associated with these cell lines.

Animals and other organisms

Policy information about [studies involving animals](#); [ARRIVE guidelines](#) recommended for reporting animal research

Laboratory animals	As reported in the Methods section ("Animals and cells"), female C57 BL/6 mice (4-8 weeks) were obtained from Jackson Laboratory Inc. and Charles River Laboratories Inc. ifn- α /Br $^{-/-}$, mavs $^{-/-}$, stinggt/gt, myd88 $^{-/-}$, cgas $^{-/-}$ and Ail4D (B6. Cg-Gt(ROSA)26Sortm14(CAG-tdTomato)Hze/J) (4-8 weeks) mice were purchased from the Jackson Laboratory and housed in an MIT animal facility
Wild animals	The study did not involve wild animals.
Field-collected samples	The samples did not involve samples collected from the field.
Ethics oversight	All animal procedures were performed with ethical compliance and approval by the Massachusetts Institute of Technology Committee on Animal Care (CAC)

Note that full information on the approval of the study protocol must also be provided in the manuscript.

Flow Cytometry

Plots

Confirm that:

- The axis labels state the marker and fluorochrome used (e.g. CD4-FITC).
- The axis scales are clearly visible. Include numbers along axes only for bottom left plot of group (a 'group' is an analysis of identical markers).
- All plots are contour plots with outliers or pseudocolor plots.
- A numerical value for number of cells or percentage (with statistics) is provided.

Methodology

Sample preparation	As described in the Methods section in detail, briefly, fresh tissues (lymph nodes, skins or tumors) were removed and digested in a medium containing collagenase D (1mg/mL) and Dnase (20 ug/mL) for 40 min at 37 °C. The cell suspensions were then filtered through a 70 μ m cell strainer and centrifuged. The cells were resuspended at 4 °C in staining buffer for 30 min at 4 °C
Instrument	Listed in the Methods section: BD LSR II flow cytometer , (BD Biosciences, San Jose, CA, USA).
Software	Collection: FACS DIVA and Analysis: FloJo.
Cell population abundance	Sorting was not done. However, for FACS gating analysis: cell populations of interest (ie., lymphocytes) were incredibly abundant (collected as much as possible from the samples ~1000,000, based on sample source).
Gating strategy	Gating strategies are referred to those described in the BD website (https://www.bio-rad-antibodies.com/flow-cytometry-gating-strategies.html). Gating was first based on FSC/SSC together with viability dyes and singlet populations. The cell populations within the gate were further analyzed based on expression of markers. Single positive staining and FMO (fluorescence minus 1) were used to determine the "true" positive. Gating was then based on positive level (after proper compensation).

- Tick this box to confirm that a figure exemplifying the gating strategy is provided in the Supplementary Information.